Enhanced capacity of fluoride scavenging from contaminated water by nano-architectural reorientation of cerium-incorporated hydrous iron oxide with graphene oxide

Kankan Mukhopadhyay[1] · Uday Chand Ghosh[2] · Palani Sasikumar[2]

Abstract

An in situ wet chemical deposition method has been applied for the successful surface modification of Ce (IV)-incorporated hydrous Fe(III) oxide (CIHFO) with a hydrophilic graphene precursor, graphene oxide (GO). The surface area of as-prepared composite (GO-CIHFO) has enhanced (189.57 $m^2\,g^{-1}$) compared with that of pristine CIHFO (140.711 $m^2\,g^{-1}$) and has irregular surface morphology consisting of microcrystals ($\sim$ 2–3 nm) and mesoporous (3.5486 nm) structure. The GO-CIHFO composite shows enhanced fluoride scavenging capacity (136.24 mg F g^{-1}) than GO (3 mg F g^{-1}) and pristine CIHFO (32.62 mg F g^{-1}) at pH 7.0. Also, in acidic pH range and at 323 K temperature, the Langmuir capacity of as-prepared composite is 190.61 mg F g^{-1}. It has been observed that fluoride removal by GO–CIHFO occurs from solutions obeying pseudo-second-order kinetics and multilayer adsorption process. The film/boundary layer diffusion process is also the rate-determining step. The nature of the adsorption reaction is reasonably spontaneous and endothermic in thermodynamic sense. It was observed that 1.2 $g.L^{-1}$ of GO-CIHFO dosage can effectively optimise the fluoride level of natural groundwater samples (9.05 mg L^{-1}) to the desirable permissible limit. Reactivation of used material up to a level of 73.77% with a solution of alkaline pH has proposed reusability of nanocomposites ensuring sustainability of the proposed material as fluoride scavenger in future.

Keywords Iron–cerium oxide · Graphene oxide · Fluoride · Field validation · Reusable

Introduction

For the last few decades, geo-environmental scientists at large are deeply alarmed by the growingly precarious threat allied with the elevated level of fluoride in groundwater, causing 'fluorosis' especially in countries like India, Bangladesh, and Sri Lanka. The World Health Organization (WHO), considering the annoying trend of fluoride poisoning in and around the world, fixed up the optimum fluoride level in drinking water at 1.5 mg L^{-1}, but diversified geological, climatological, and topographical patterns have aggravated the occurrence of fluoride in drinking water (G. Alagumuthu and Rajan 2008; Chakrabarti and Bhattacharya 2013). Several techniques have been adopted to reach a desirable level of fluoride concentration in drinking water (Meenakshi and Maheshwari 2006; Jagtap et al. 2012). Among them, surface adsorption has been receiving special attention over researchers due to its easy operation, low energy consumption, cost effectiveness, and treatment efficiency at low concentrations of contaminants (lower than 100 mg L^{-1}), making it an ideal medium for use even in rural areas (Bhatnagar et al. 2011).

To date, composites of many oxides and hydroxides of several metals have been developed for the adsorptive removal of fluoride from aqueous solutions, such as iron, aluminium, silica, calcium, magnesium, chromium, titanium, zirconium, cerium, and lanthanum (Biswas et al. 2009, 2010; Liu et al. 2010; Deng et al. 2011; Chen et al. 2012; Tomar et al. 2013; Basu and Ghosh 2013; Barathi et al. 2013; Ghosh et al.

✉ Palani Sasikumar
sasikumar.chem@presiuniv.ac.in

[1] Department of Geology, Presidency University, 86/1 College Street, Kolkata 700073, India

[2] Department of Chemistry, Presidency University, 86/1 College Street, Kolkata 700073, India

2014; Zhang et al. 2015; Zhu et al. 2015; Chen et al. 2016a, b; Mukhopadhyay et al. 2017a), and have been reported as efficient adsorbents for fluoride removal. Even though rare-earth metal (Ce, La, Zr) oxides show very good adsorption efficiency with fluoride, their high cost restricts them in real application. We overcome the high cost of Ce without loss of their F^- absorption efficiency by introducing Ce(IV) ion into hydrous Fe(III) oxide. Accordingly, we reported the synthesis of Ce(IV)-incorporated hydrous Fe(III) oxide (CIHFO) and its application for fluoride adsorption from water at neutral pH (Mukhopadhyay et al. 2017a). Now, we are aiming to enhance the adsorption efficiency towards fluoride by modifying the surface of the CIHFO component.

Improvement of the adsorption capacity of these oxides by surface modification has also brought about promising output, and now, most of global research is swinging towards the deployment of surface-amended materials and their diversified application, particularly in water purification. In this context, several methods have been adopted for modifying the surface and properties of metal oxide nano-composite (NC); these include (i) introducing a new metal atom into the binary metal oxide component, or directly synthesising the ternary metal oxide NC, to modify the surface to enhance their property (Biswas et al. 2010; Zhao et al. 2012a; Tang and Zhang 2016; Mukhopadhyay et al. 2017a); (ii) introducing carbon-based materials such as carbon nano-tubes, activated charcoal, graphene, and graphene oxide (Li et al. 2011; Barathi et al. 2014; Mohan et al. 2016a; Kanrar et al. 2016; Kuang et al. 2017); (iii) calcination of the binary metal oxide with different temperatures (Deng et al. 2011; Mukhopadhyay et al. 2017a); and (iv) changing the solvent of preparation leads to the modified surface of the material (Chen et al. 2012; Zhang et al. 2015, 2017). At this moment, we adopted the second method, i.e., introduction of the carbon-based material to binary oxides.

Graphene and its derivatives have received great attention in recent years. Graphene oxide (GO), the precursor of graphene, is a non-stoichiometric compound with a variety of compositions that emanates from synthesis conditions. GO is characterised by high water dispersibility, strong acidity, low electrical conductivity, and presence of functional groups that exhibit high affinity for basic compounds, anions, and cations. It is densely packed with oxygen-containing and hydrophilic groups, such as hydroxyl, epoxide, carboxyl, and carboxylic groups, that enhance the adsorptive property of GO. Graphene and graphene oxide have been already reported as effective adsorbents for the adsorption of fluoride with an uptake capacity of 35.59 and 3 mg F g^{-1} respectively (Li et al. 2011, 2013). Graphene oxide (GO) acts as an excellent host for nanoparticles (NPs), and integration of NPs of iron, aluminium, cerium, zirconium, lanthanum oxide etc. inside the honeycomb lattice of GO/rGO accentuates the adsorption efficiency and makes these NCs a promising medium for fluoride removal (Barathi et al. 2014; Mohan et al. 2016a; Kanrar et al. 2016; Kuang et al. 2017). This feature can be beneficial to entrap and remove impurities from aqueous solution through the formation of insertion complexes with GO and metal NCs. This article entails adsorptive marvels of GO–Ce/Fe hydrous oxide (GO–CIHFO), where an iron–cerium hybrid oxide (Fe/Ce = 1.0:0.5) surface has been attempted to be modified in a delicate manner with GO so that functional groups of GO (hydroxyl, epoxide, carboxyl, and carboxylic groups) may potentially provide structural firmness with the generation of a metal oxide–GO NC. Accordingly, we prepared GO-incorporated Ce(IV)-incorporated hydrous Fe(III) oxide (GO–CIHFO), which shows enhancement of fluoride absorption capacity as anticipated. Furthermore, the newly developed material has been established as a NC by some modern analytical tools viz. powder X-ray diffraction (XRD), X-ray photoelectron spectroscopy (XPS), transmission electron microscopy (TEM), scanning electron microscopy (SEM), optical microscopy (OM) and Fourier transform infrared (FTIR) spectroscopy, thermo-gravimetric analysis (TGA), and differential thermal analysis (DTA). The effects of various process parameters like pH, adsorbent dose, fluoride concentration variation, temperature, and contact time upon the overall adsorption process were also carried out to explore the adsorption mechanism. Finally, the fluoride extraction capacity of the proposed material has been validated with natural fluoride-enriched groundwater samples.

Materials and Methods

All reagents, preparation of fluoride solution and fluoride analysis, instrumental details applied for the characterisation of material, and theoretical particulars used in this research work are also provided in details in the "Supporting information (SI)" section.

Preparation of Graphene Oxide

Synthesis of GO was based on the modified Hummer's method (Hummers and Offeman 1958). In this study, an exactly known amount of graphite flakes (3.0 g) was mixed with 50% weight amount of $NaNO_3$ (in present experiment, 1.5 g) and concentrated H_2SO_4 (75 mL, generally 25 times higher than the volume of graphite weight amount) was added to the mixture and stirred it at 0 °C in ice bath. For 6 h of experiment, $KMnO_4$ (9.0 g) was added in portions after a certain interval under vigorous stirring so that the temperature should not exceed 20 °C. A pasty light brownish mixture was developed and then additional $KMnO_4$ (9.0 g) was added to it and stirred for 12 h at room temperature.

Then 300 mL of ice-chilled distilled water was added slowly to the mixture followed by drop-wise addition of 30% H_2O_2

to reduce the excess $KMnO_4$ to control further oxidation. With the passing of time as the reaction continued, the suspension turned brown to light yellow. This mixture was sequentially washed with 5% of HCL and warm water thoroughly to remove impurities and the obtained mass was dried and dispersed in distilled water. After that, it was centrifuged at 5000 rpm for 30 min to remove large heavy particles. The supernatant was filtered through a 0.45-μm pore size membrane and washed with 50% ethanol to isolate the graphene oxide mass and was dried under vacuum at 60 °C and pure GO as a brownish-black solid product as collected.

Preparation of Ce (IV)-incorporated hydrous Fe (III) oxide

The method of CIHFO preparation was discussed elaborately elsewhere (Mukhopadhyay et al. 2017b). In brief, a measured volume of ferric chloride (0.1 M) solution in (0.1 M) HCl and ammonium ceric nitrate (0.05 M) in (0.1 M) HNO_3 were mixed together and ammonia solution (mixture of 25% ammonia solution and 0.1 M ammonium carbonate solution) was added into the mixture drop-wise in a controlled manner to increase the mixture pH to ~ 6.0–7.0. Both the metal, iron (III), and cerium (IV) were hydrolysed and precipitated as mixed hydroxide gel. The brownish-yellow filtered residue was washed and oven dried at 75 °C (± 5 °C) to convert it to hydrated oxide mass.

Preparation of graphene oxide-associated Ce (IV) -incorporated hydrous Fe(III) oxide

Graphene oxide of a different qualitative mass weight percentage of prepared GO (Table-S1) was taken separately in Erlenmeyer flasks and sonicated for ~ 30 h in mixed solution (1:1 *v/v*) of (0.1 M) ferric chloride in (0.1 M) HCl and (0.05 M) ammonium ceric nitrate in (0.1 M) HNO_3 for complete dispersion. Then, pH of the mixture with well-dispersed GO suspension was increased to ~ 6.0–7.0 by drop-wise addition of ammonia solution (mixture of 25% ammonia solution and 0.1 M ammonium carbonate solution) in this mixed solution. Blackish-brown jelly-like precipitated mass was kept as such with the mother liquid overnight and then filtered and washed simultaneously with de-ionised water and oven dried at 50–55 °C. Finally, the composite was crushed and sieved to obtain the desired particle size (140–290 μm) and kept for further analytical experiments.

Batch adsorption study

A systematic batch adsorption study is an essential step to establish an adsorbent as a good water purifier. To achieve this goal, a measured volume fluoride solution (50 mL) with a desired initial fluoride concentration (C_i, mg L^{-1}) was taken in 250-mL polyethylene (PE) bottle along with a definite mass (0.01 g) amount of GO-CIHFO (except dose variation study) and agitated at 250 (± 5) rpm using a thermostatic shaker for two hours (except time-dependent experiment). The filtrate obtained by immediate filtration process was analysed to evaluate residual concentration of fluoride (C_f, mg.L^{-1}).

pH of any solution is considered a crucial parameter that has an immense impact upon any adsorption process. In the present batch study, the effect of the solution pH upon fluoride adsorption was explored independently in the pre-programmed pH$_i$ 3.0 to 10.0 by a unit increment, with two different fluoride solutions (C_i: 5.0 and 15.0 mg.L^{-1}). The pH value of each test solution was adjusted with 0.1 M HCl and/ 0.1 M NaOH solution, as required, respectively.

Reaction kinetics for fluoride adsorption by GO–CIHFO were conducted with three separate concentrations of fluoride solution. The same experiment was also carried out in three different temperatures (288 K, 303 K, and 313 K) with a fixed fluoride concentration (15.0 mg L^{-1}).

For equilibrium experiments, fluoride solution (C_i) ranged between 5.0 and 60.0 mg L^{-1} was taken for scheduled experiments at four temperatures, 288 K, 303 K, 313 K, and 323 K respectively, agitation time (2 h), and speed 250 (± 5) rpm. The fluoride concentration at equilibrium (C_e, mg L^{-1}) was analysed by ion-selective electrode and equilibrium capacity (Q_e, mg g^{-1}) was calculated. Thermodynamic parameters ($\Delta S°$, $\Delta H°$, $\Delta G°$) were evaluated from the results of equilibrium analysis.

Groundwater may also contain some ions like HPO_4^{2-}, SO_4^{2-}, HCO_3^-, NO_3^-, and Cl^-. Adsorption of fluoride over tuned GO–CIHFO may be influenced by the presence of such ions. To evaluate the effects of these ions upon fluoride adsorption, batch experiments were conducted at neutral pH using the fluoride solution of $C_i = 10.0$ mg L^{-1} in the presence of different concentration levels of competing ions.

Adsorption capacity

Immediately after each experiment, the adsorbent particles were filtered through a 0.45-μm membrane filter. The residual fluoride level left in each filtrate was analysed. The adsorbed amount of fluoride by GO–CIHFO was calculated by application of the following mass balance equation(Mukhopadhyay et al. 2017b)

$$Q_e = (C_i - C_f) \times \frac{V}{M} \tag{1}$$

where Q_e is the adsorption capacity (mg g^{-1}), V the volume of solution (L), and M is the mass of adsorbent (g) used to carry out the batch experiments. The significance of C_i and C_f have been given previously.

The removal percentage of fluoride by adsorbate was calculated as follows (Podder and Majumder 2016):

$$Re(\%) = \frac{(C_i - C_f)}{C_i} \times 100 \qquad (2)$$

Desorption and reuse

For desorption study, fluoride adsorbed GO–CIHFO was prepared first agitating the material with an initial fluoride concentration of 60 mg L^{-1}. Fluoride adsorbed GO–CIHFO was then kept for air drying which was used to desorption study. The reagents used as fluoride scavenger from the solid matrix were pH-adjusted (8.0, 9.0, 10.0, 11.0, 12.0, and 13.0) distilled water. After achieving the optimum pH level for defluoridation, fluoride-adsorbed GO–CIHFO was defluoridated and the defluoridated solid matrix was carefully collected and used to repeat the aforesaid adsorption–desorption study (Wen et al. 2015; Mohan et al. 2016b). The adsorbents were reused for five cycles in this study. Mass balance equations used for desorption and regeneration process (Zhao et al. 2012b) are mentioned in Eqs. (3)–(4).

- Desorption study

$$\frac{The\ amount\ of\ Fluoride\ Desorbed}{The\ amount\ of\ Fluoride\ Adsorbed(same\ cycle)}\ X\ 100 \qquad (3)$$

- Regeneration and recycling

$$\frac{The\ amount\ of\ Fluoride\ adsorbed\ (Reuse)}{the\ amount\ of\ Fluoride\ adsorbed\ (the\ first\ cycle)}\ X\ 100$$
$$(4)$$

Field validation

The purpose of this study is to develop an adsorbent that can be used as water purifier. In this context, field validation with optimised material is an essential step. To achieve this goal, water samples have been collected from different hand pump-attached tube wells of Kashipur block, the most adversely fluoride-affected region of Purulia district, under the state of West Bengal, India. The fluoride concentration of collected water samples was analysed in the laboratory by ion-selective electrode and water sample with maximum fluoride concentration (Kharai village) was used for field validation (Mukhopadhyay et al. 2017b).

Theory

Kinetics studies

Adsorption of any pollutant over any adsorbent is time dependent. The physico-chemical nature of the adsorbent also influences the overall adsorption process. Kinetics modelling for the batch adsorption process is considered a very crucial aspect as it helps in determining the adsorption mechanism and also helps in exploring the rate-determining step of the ongoing adsorption process. In the present batch study, pseudo-first order, pseudo-second order, mass transfer, intra-particle diffusion, the Elovich model, and the Richenberg model were applied to study different kinetics parameters.

Pseudo-first order model

The non-linear form of the pseudo-first order model (PFO) kinetic equation can be expressed as follows:

$$Q_t = Q_e\{1 - \exp(-k_1.t)\} \qquad (5)$$

where Q_e and Q_t are the amounts of a solute adsorbed per unit weight of adsorbent (mg g^{-1}), i.e. the adsorption amount at equilibrium and at time t (min), respectively, and k_1 stands for the PFO rate constant (Biswas et al. 2009; Ghosh et al. 2014; Mukhopadhyay et al. 2017).

Pseudo-second order model

The non-linear expression of PSO kinetic equation can be expressed as follows:

$$Q_t = \frac{(t.k_2.Q_e^2)}{\{1 + (t.k_2.Q_e)\}} \qquad (6)$$

Here, k_2 stands for PSO rate constant and others have the same meaning as above (Biswas et al. 2009; Ghosh et al. 2014; Mukhopadhyay et al. 2017a, b).

Mass transfer

The extent of removal of any pollutant by adsorption process is highly influenced by a wide range of contaminants which transfer from the bulk solution to the surface of the solid adsorbent and at the interface of particular adsorbent or at the interface of liquid and solid particles. For the present study, this probability was examined based on the model described by Mckay et al. 1981.

$$\ln\left(\frac{C_t}{C_i} - \frac{1}{1+mk}\right) = \ln\left(\frac{mk}{1+mk}\right) - \left(\frac{1+mk}{mk}\right)\beta_1 S_s t \quad (7)$$

Here, C_i and C_t signify the solute concentration (mg L^{-1}) at time (min) t = zero and any time, t, respectively. The m denotes adsorbent mass per unit volume (g L^{-1}), k is the Langmuir constant, and S_s is the specific surface area of adsorbent per unit volume of the reaction mixture (cm^{-1}). β_1 stands for the coefficient of external mass transfer (cm^2 s^{-1}). Values of β_1, the coefficient of mass transfer, were calculated at different values of temperature by the slopes and intercepts of the plots of "ln $[C_t/C_i - 1/(1 + mk)]$ versus t (Sharma and Weng 2007; Singh et al. 2016)

The general mechanism thought to be involved in mass transfer is:

1. Gentle movement of the pollutant from the bulk solution to the upper boundary of adsorbent.
2. Slowly diffusion of adsorbate from the boundary film layer to the surface of adsorbent.
3. Adhesion of the adsorbate into the internal pore and spaces in between the active sites of the adsorbent.
4. Simultaneous adsorption and desorption of the adsorbate at the active sites of the adsorbent surface.

From the above points, it can be said that in the first step, adsorption might occur in hydro-dynamic conditions that obstruct the concentration gradient in between the solution and boundary film. So, from this point of view, it cannot be a rate-limiting step. Hence, external diffusion (step 2) or intra-particle diffusion, will be the slowest step that may be considered the rate-controlling step (RDS) of the proposed adsorption process (Mohan et al. 2016a, b).

Intra-particle diffusion model

In an ongoing adsorption process, there is an always a fair chance of diffusion of adsorbate into the pores of the adsorbent which is often considered RDS of the particular adsorption process. The intra-particle diffusion (IPD) rate constant (k_{id}) at different concentrations and in temperatures can be determined by the Weber–Morris model (Biswas et al. 2009; Ranjan et al. 2009) that can be expressed as follows:

$$Q_t = k_{id} t^{0.5} + C \quad (8)$$

where Q_t is the quantity of adsorbate (mg g^{-1}) adsorbed at time t (min), k_{id} is the initial rate of IPD calculated by the slope of the plot of Q_t vs. $t^{0.5}$ (mg.L^{-1} min$^{-0.5}$) and C, is the y-intercept which gives proper information all about the boundary layer thickness (Banerjee and Chattopadhyaya 2017). This observation was further proved by the value of the IPD

coefficient (D), which can be calculated by the following equation.

$$D = \frac{0.03 r^2}{t^{0.5}} \quad (9)$$

where r (cm) stands for the average radius of the adsorbent particle and $t^{0.5}$ (min) is the time required for half of the adsorption (Biswas et al. 2009; Mohan et al. 2016a, b).

Elovich model

This equation is more familiar to determine chemisorption kinetics of any gas on the heterogeneous surface of any adsorbent. Presently, this equation has been widely applied to evaluate the adsorption nature of any adsorbate from an aqueous medium. The equation mentioned is as follows:

$$\frac{dQ_t}{dt} = a \exp(abQ_t) \quad (10)$$

where a signifies the rate of chemisorption at zero coverage (mg/(g/min)) and b implies the extent of surface occupancy and activation energy required for chemisorption (g/mg). These are obtained from the slope and intercept of the plots of Q_t vs. ln (t) (min).

$$Q_t = \frac{1}{b}\ln(ab) + \frac{1}{b}\ln\left(1 + \frac{1}{ab}\right) \quad (11)$$

This equation is the integrated form of Eq. 10 with an assumption that $Q_t = 0$, $t = 0$ as the lower of limit of integration. If the value of t is much higher, i.e. $t > 1/ab$, the plots of Q_t vs. ln (t) should be linear (Ranjan et al. 2009).

Richenberg model

The Richenberg expression can be used to distinguish between the film diffusion and the IPD, which can be given by the following equation:

$$G = 1 - \frac{6}{\Pi^2}\exp(-\beta_t) \quad (12)$$

where $G = Q_t/Q_e$ and β_t is the mathematical function of G, which can be calculated from the respective value of G by the following equation:

$$\beta_t = -0.4977 - \ln\left(1 - \frac{Q_t}{Q_e}\right) \quad (13)$$

The β_t values at different contact times (t) can be calculated using the above equation (Eq. 13). The calculated β_t values were plotted against time t (min), and the slope was used for the calculation of factor β_t. The effective diffusion coefficient

D_i (cm^2 s^{-1}) has been calculated using the value of factor β_t from the following equation.

$$\beta_t = \frac{\varPi D_i}{r^2} \qquad (14)$$

where adsorbent particles were assumed to be spherical and r is assumed as the radius of the adsorbent particles. The obtained values of D_i will be thus useful to decide the process whether it is IPD or external diffusion. If plots are straight lines passing through the origin, then the adsorption process is governed by particle diffusion mechanisms; otherwise, both external diffusion and IPD jointly determine the rate of adsorption (Hamayun et al. 2014; Mohammadian et al. 2016; Mohan et al. 2016a, b; Singh et al. 2017). Values of film diffusion (D_1) and pore diffusion (D_2) also can provide information regarding the mechanism of adsorption whether it is kinetically influenced by film or pore diffusion. D_1 and D_2 can be determined by the application of the following equations (Hamayun et al. 2014).

$$\frac{Q_t}{Q_e} = 6\left(\left(\frac{D_1}{\varPi a^2}\right)^{0.5}\right)t^{0.5} \qquad (15)$$

$$ln\left(1 - \frac{Q_t}{Q_e}\right) = ln\frac{6}{\varPi^2} - \left(\frac{D_2 \varPi^2}{a^2}\,t\right) \qquad (16)$$

D_1 is calculated from the slope of the plot of Q_t/Q_e vs. $t^{0.5}$ and D_2 is calculated from the plots of ln $(1 - Q_t/Q_e)$ vs. t for fluoride adsorption on GO–CIHFO (Hamayun et al. 2014).

Isotherm models

Isotherm modelling of any adsorption process is an essential step to determine the distribution pattern of any adsorbate between the solid and liquid phases at equilibrium. Hence, to establish the adsorption efficiency of a newly developed adsorbent, optimisation of a particular adsorption study with an appropriate isotherm model is considered a basic requirement for commercialization of the prepared adsorbate. To achieve the goal of the present study, three isotherm models were applied, namely Langmuir, Freundlich, and Dubinin–Radushkevich (D–R) isotherms. Langmuir and Freundlich are two basic fundamental isotherm models most widely applied to evaluate equilibrium data of any adsorption process. Meanwhile, the D–R isotherm envisaged the nature of the adsorption process.

Langmuir isotherm

According to the Langmuir model, each adsorbate molecule retains the same adsorption energy. All active sites pose equal attraction towards adsorbate and there is no internal interaction between molecules; hence, this isotherm denotes a homogeneous adsorption process. A non-linear form of Langmuir isotherm is expressed as follows:

$$Q_e = \frac{Q_m K_l C_e}{[1 + K_L C_e]} \qquad (17)$$

where C_e (mg L^{-1}) and Q_e (mg g^{-1}) are the fluoride concentration and adsorption capacity at equilibrium. The Q_m (mg g^{-1}) is the maximum monolayer adsorption capacity (mg g^{-1}) and K_L (L mg^{-1}) the equilibrium constant related to the net enthalpy change of the reaction (Biswas et al. 2009; Ghosh et al. 2014; Mukhopadhyay et al. 2017a, b).

Freundlich isotherm

The Freundlich model assumes the non-ideal multilayer adsorption that is generally associated with the heterogeneous surface of adsorption sites. The non-linear expression of Freundlich can be set as:

$$Q_e = K_F \times C_e^{1/n} \qquad (18)$$

where the K_F is the Freundlich adsorption capacity and $1/n$ is an empirical constant related to the adsorption intensity (Mukhopadhyay et al. 2017a, b).

Dubinin–Radushkevich isotherm

The Dubinin–Radushkevich (D–R) isotherm was elucidated to estimate the free energy of reaction and can be obtained from the equilibrium isotherm data to predict the nature of adsorption. The linear form of this isotherm is written as:

$$lnQ_e = lnQ_m - \beta E^2 \qquad (19)$$

where E is the Polanyi potential and can be extracted from Eq. (17) below:

$$E = RT \ln\left(1 + \frac{1}{C_e}\right) \qquad (20)$$

The plots of the ln Q_e against E^2 become a straight line and the values of slope and intercept of the plot was used to calculate the value of β and Q_m, Q_e, and Q_m are equilibrium and maximum D–R adsorption capacities in (mol kg^{-1}), respectively, and β is signifying that the activity coefficient is mainly related with the mean free energy (E_{DR}) of the reaction as per the following equation:

$$E_{DR} = 1/(-2\beta)^{1/2} \qquad (21)$$

Depending on the obtained value of E, the nature of adsorption (physisorption, ion-exchange, or chemisorption) can

be determined (Mohan et al. 2016a, b; Mukhopadhyay et al. 2017a, b).

Results and discussion

Characterisation of GO–CIHFO

FTIR analysis

Fig. S1(A-B) has been represented by the FTIR spectra of prepared GO and GO–CIHFO, whereas fluoride-adsorbed GO–CIHFO has been recorded in Fig. S2. The stretching and the bending modes of vibrations for the O–H bond had been indicated by the band at wave number (ν) 3000–3500 cm^{-1} and $\sim$ 1600–1650 cm^{-1}, presented on the surface of the nanocomposite, respectively. The peaks observed at 3417.13 cm^{-1} and 1384.79 cm^{-1} described firmly the association of C–OH into the matrix of graphite during oxidation. Adsorption bands of 2923.88 cm^{-1} and 2857.03 cm^{-1} denote the ν_{sym} and ν_{asym} stretching vibration mode of CH$_2$ (Barathi et al. 2014). In FTIR spectrum of GO (Fig. S1A), the bands at wave number 1751 cm^{-1} and 1729 cm^{-1} are the stretching bands for C=O (monomer H bonded) and C=O (dimer H bonded).The band peaks at 1190 cm^{-1}, 1063 cm^{-1} are due to the presence of epoxy C–O and alkoxy C–O stretching vibration present in prepared GO and confirmed the formation of graphene oxide (GO). After incorporation of GO into CIHFO, the band at 3417.13 cm^{-1} shifted to 3380.46 cm^{-1} and broadened up ensuring the interaction of metal ions with the hydroxyl group of GO and further surface enhancement of CIHFO. The characteristic band observed at 414.67 cm^{-1} and 983.63 cm^{-1} can be attributed to Fe–O and Ce–O bonds. Significant modification of peak intensity has been observed after fluoride adsorption. Shifting of bands from 3417.13 to 3243.04 cm^{-1} and from 1633.59 to 1625.88 cm^{-1} attributed with the interaction of fluoride ions with surface hydroxyl groups of the adsorbent (Fig. S2).

XRD pattern study

Dramatic changes in crystalline phases and in crystallite size have been observed with incorporation of one material to another material. XRD is the most advanced technical tool that helps to identify such changes. Figure 1 represents the XRD patterns of (a) GO, (b) GO–CIHFO for comparison. The diffraction peaks for graphite at 2θ = 26.38° and 54.54° corresponding to the plane (002) and (004) respectively was totally diminished [36] and the most evident diffraction peak at 2θ = 10.82° observed with the corresponding d-spacing of 0.424 nm with a full width half maximum (FWHM) at $\sim$

0.82. The d-spacing is expanded wisely as compared with pristine graphite (0.34 nm) suggesting that graphite is fully oxidized to GO (Mohan et al. 2016a). The disappearance of the characteristic diffraction peaks associated with graphite suggests the presence of carboxyl and hydroxyl functional groups in GO during exfoliation resulting to the oxidation of graphite layers (Barathi et al. 2014). In prepared GO–CIHFO, the characteristic peak of GO not having been observed might be due to complete interaction of GO with CIHFO. The XRD pattern of the GO–CIHFO (Fig. 1b) showed the presence of peaks at °2θ = 28.85, 33.25, 35.05, 47.74, and 56.74 indicating the signature of CIHFO (Mukhopadhyay et al. 2017a). Full width half maximum (FWHM) at $\sim$ 1.89–0.67 revealed the presence of microcrystalline particles and crystallites of $\sim$ 5–10 nm in size.

TG/DTA analysis

TG and DT analyses are the most authentic measurements to determine the thermal stability of the proposed material. Hence, TGA and DTA of GO–CIHFO gave a glimpse of temperature-dependent stability characteristics of the proposed material. The TG spectrum of GO–CIHFO shows a rapid but smooth loss of mass ($\sim$ 35% of initial mass) up to a temperature $\sim$ 435 °C (Fig. 1c). This weight loss assumed to be associated with removal of surface abandoned water molecules and hydroxyl groups by dehydroxylation of GO-incorporated hydrous mixed oxide nanocomposite(Kanrar et al. 2016) and removal of carbon and oxygen in the form of CO from the composite. A sharp endothermic peak of DTA spectrum (Fig. 1d) observed at 80 °C ensures the loss of physically adsorbed water molecules from the surface of the hydrous nanocomposite. A sharp but small exothermic peak at 260 °C indicates thermal conversion of GO and a broad DTA exothermic peak at above $\sim$ 350 to $\sim$ 435 °C is closely associated with the phase transition of the material. No occurrence of any other bands above 500 °C justifies that the residue of the nanocomposite is thermally stable within the studied temperature range.

Optical microscope and SEM imaging with EDX

The images (Fig. S3) obtained from optical and scanning electron microscopic analyses ensure the irregular surface morphology GO–CIHFO. Irregular-shaped agglomerated particles are encapsulated within the layers of GO and act as a scaffolding surface for CIHFO. The SEM–EDX spectrum (Fig. S4) has also supported the presence of higher carbon and oxygen content with respect to cerium and iron metal oxides. This is also fulfils our purpose to use GO as a surface modifier to develop a cheaper adsorbent rather than CIHFO, the pure mixed metal oxide. From the analytical data, the
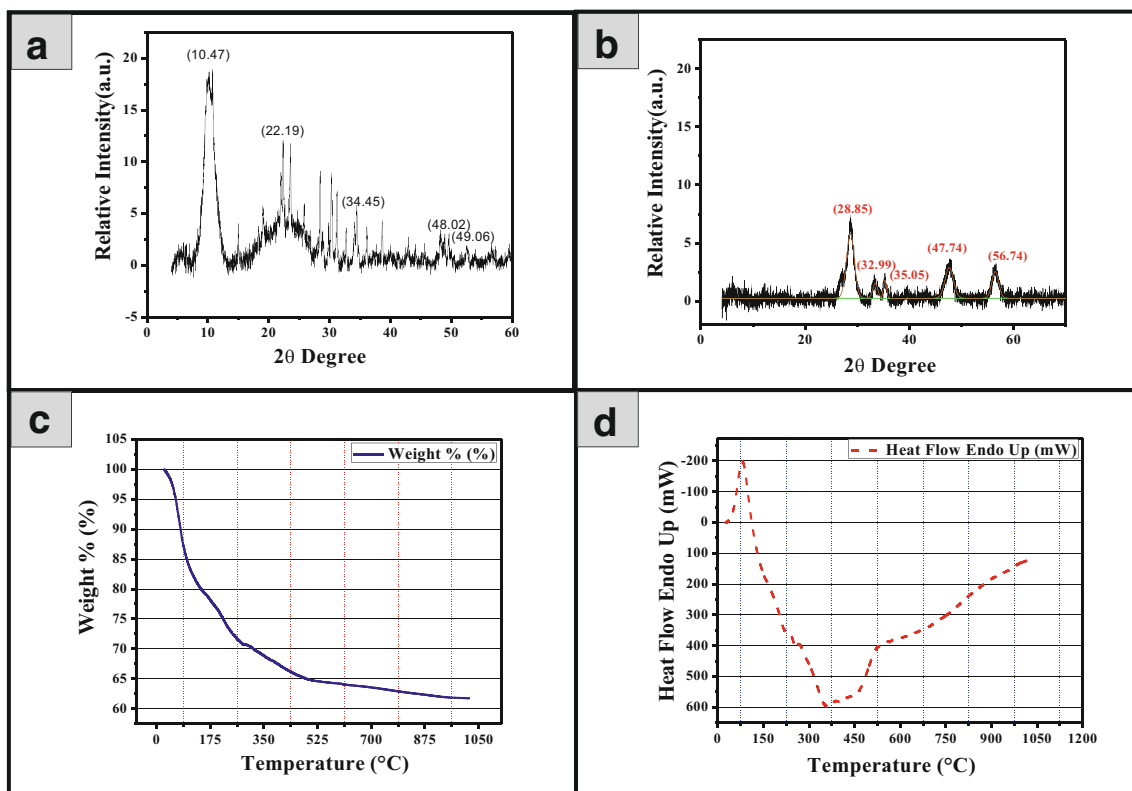
Fig. 1 **a** The powder X-ray diffraction patterns of GO. **b** The powder X-ray diffraction patterns of GO–CIHFO. **c** Thermogravimetric (TG) analysis of GO–CIHFO. **d** Differential Thermal (DT) analysis of GO–CIHFO

empirical formula of GO-incorporated mixed hybrid oxide is established as $Fe_{0.279}$ $Ce_{0.198}$ $C_{0.222}$ $O_{3.36}$.

TEM imaging

Transmission electron microscopy (TEM) is used to visualise the inner structure of particles and the size of the prepared nanocomposite. Figures 2 and 3 represent the TEM images of GO–CIHFO with EDX spectrum and elemental mapping. Figure 2a–c show agglomerated fine particles of GO–CIHFO in addition with the broken sheet of GO. Overlapping of figure print-like structures (Fig.2b) in high resolution strengthens the degree of agglomeration of GO–CIHFO and anchoring of metal oxides in GO layers. Figure 2d and e also revealed the microcrystalline nature of the proposed material with an average particle size ~ 2–3 nm. High agglomeration might be due to the incorporation of metal oxides into the GO layers. TEM–EDX spectrum (Fig. 3a) also supports the presence of higher carbon and oxygen content rather than iron and cerium that support the data acquired from SEM–EDX analysis. Signals for C and O along with iron and cerium suggested the incorporation of CIHFO on the GO surface. Figure 3b represents the elemental mapping analysis for C, O, Fe, and Ce also revealed that CIHFO mixed oxide

particles are evenly distributed on the surface of the GO layer.

AFM analysis

2D and 3D atomic force micrograph (AFM) images of GO-CIHFO are shown in Fig. S5A and Fig. S5B, representing the rough and undulating nature of surface morphology. To obtain the surface profile, particle size approximation and their distribution pattern, a small portion of the 2D image was further extracted. Height distribution curve and extracted profile firmly recognised that, more or less, the size of HCZMO particles was ranged 2–6 nm while particle size distribution range established that the average particle size is ~ 2.1–12 nm that supports the particle size obtained from TEM images (Fig. 2).

Raman analysis

Raman spectroscopy is another useful tool that can provide authentic structural information for carbonaceous materials such as graphene. Raman spectra exhibited two distinctive D band and G band particularly for materials of graphitic origin. The pristine graphite D band was obtained at 1351 cm^{-1} and G band at 1582 cm^{-1} (Barathi et al. 2014). Sp^3 domains of carbon layers quietly associated with D band while G band was
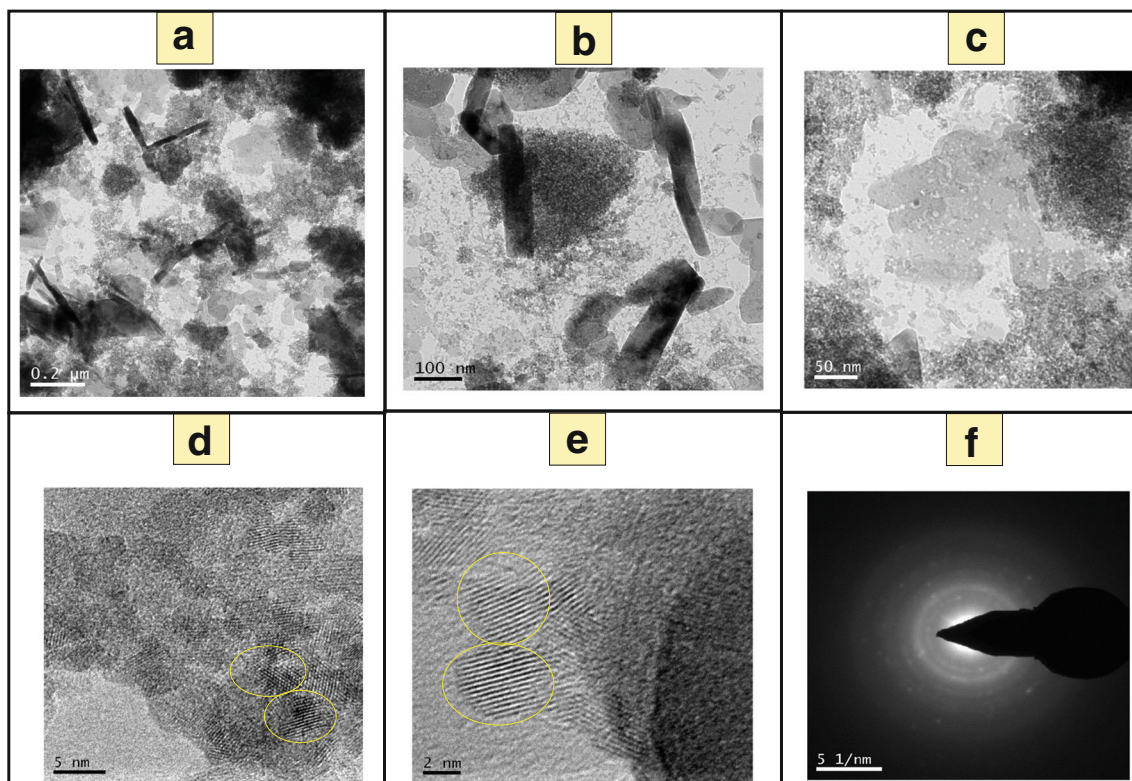
Fig. 2 **a** TEM images of GO-CIHFO (0.2-μm scale). **b** TEM images of GO–CIHFO (100-nm scale). **c** TEM images of GO–CIHFO (50-nm scale). **d**, **e** TEM images of GO-CIHFO with prominent figure print-like structure. **f** with SAED image of TEM images of GO-CIHFO (50 nm scale)

assigned to sp^2 in plane vibration pattern (Barathi et al. 2014). Figure 4a demonstrated the Raman spectra of GO, showing a prominent G band at 1592.13 cm^{-1} and a blunt D band at 1324.97 cm^{-1}. Any change in the intensity of the D band and G band are often considered an indicator to quantify the extent of disorder associated with sp^2 and sp^3 domains of carbonaceous materials. It was observed that intensity ration (I_D/I_G) decreases from 1.02 to 0.99 when GO is incorporated with the CIHFO lattice structure. Shifting of D band from 1324.97 to1305.59 cm^{-1} (lower frequency range) and G band

from1592.13 to 1601.91 cm^{-1}(higher frequency range) ensures significant alteration of both sp^2 and sp^3 domains of GO after due to chemical doping with CIHFO and successful formation of the composite (Fig. 4b).

XPS analysis

Elemental- or chemical-state determination of the prepared composite was also established further using the XPS technique. This technique irradiates the sample with X-ray
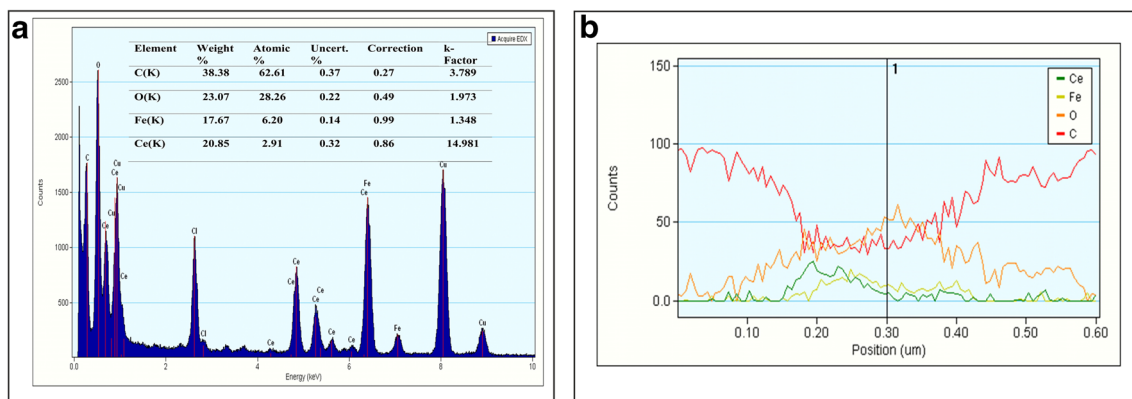
Fig. 3 **a** EDX spectrum of GO-CIHFO nano-composite including quantification results. **b** Elemental mapping of C, O, Fe, and Ce obtained from TEM analysis of GO–CIHFO
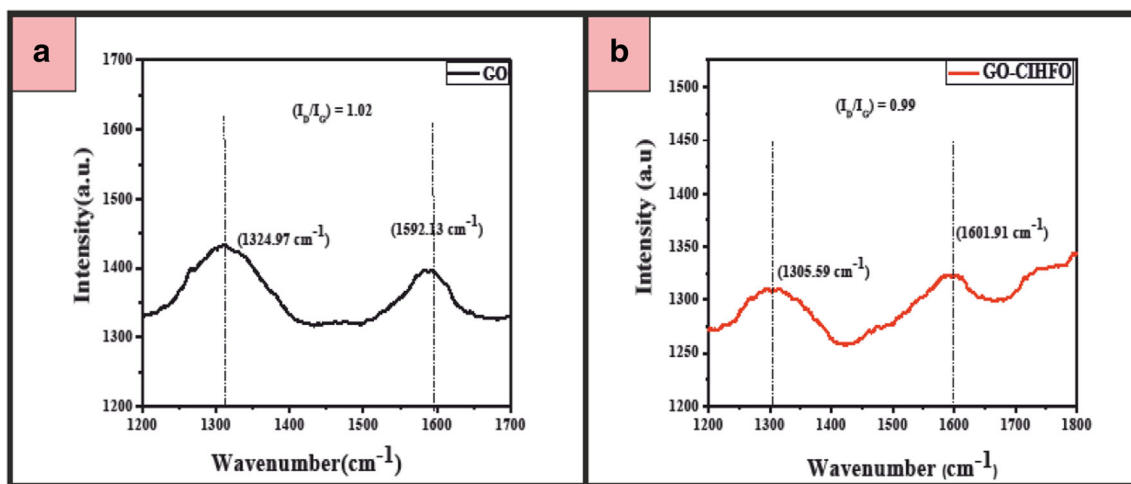
Fig. 4 **a** Raman Spectra of GO. **b** Raman Spectra of GO-CIHFO

photon and analyses the emitted core-level electron. The emitted electron has a peculiar kinetic and binding energy of the atomic orbital of a certain atom dependent on the incident X-ray. The binding energy of the emitted photo-electrons is analysed to identify the elements present (Briggs 1978). XPS of GO–CIHFO has been recorded for identify the carbon, oxygen, iron, and cerium and shown in Fig. 5. The full spectrum of composite material shown in Fig. 5a. The observed C 1s spectrum (Fig. 5b) clearly indicates the presence of GO in the composite. The peaks at 284 and 288.3 eV correspond to C–C and C=O respectively (Drewniak et al. 2016). The O 1s peak obtained between 529 (Ce^{4+}–O) and 530.5 eV ($Fe^{2+/3+}$–O) correspond to metal oxides, the spectrum further broadens up to ~533 eV (C=O) corresponds to carbonyl moiety from GO shown in Fig. 5c (Baltrusaitis et al. 2007). Further the peaks at 710 (Fe $2p_{3/2}$) (Langevoort et al. 1987; Wan and Wang 2016), 718.4 (Fe satellite), 723.6 (Fe $2p_{1/2}$) (Wan and Wang 2016), and 732.4 (Fe satellite) (Baltrusaitis et al. 2007) confirm the presence of the Fe–O component of the material (Fig. 5d). Finally, the resemblance of the presence of Ce^{4+} has been established by the Ce 3d XPS spectrum as presented in Fig. 5e, which shows peaks at 881.7, 888.9, 897.4, 900.2, 906, and 915.9 eV, corresponding to Ce^{4+}–O. An almost similar pattern of the Ce 3d XPS spectrum also has been reported by other groups of researchers (Tang and Zhang 2016).

Surface area analysis

Figure 6 describes BET analysis to determine specific surface area, pore size, and pore volume of GO–CIHFO before and after fluoride ion adsorption. The N_2 adsorption/desorption isotherm curves for both before and after fluoride ion adsorption can be acknowledged as mixed isotherm, i.e. a combination of type I and IV isotherms. Such a pattern of BET
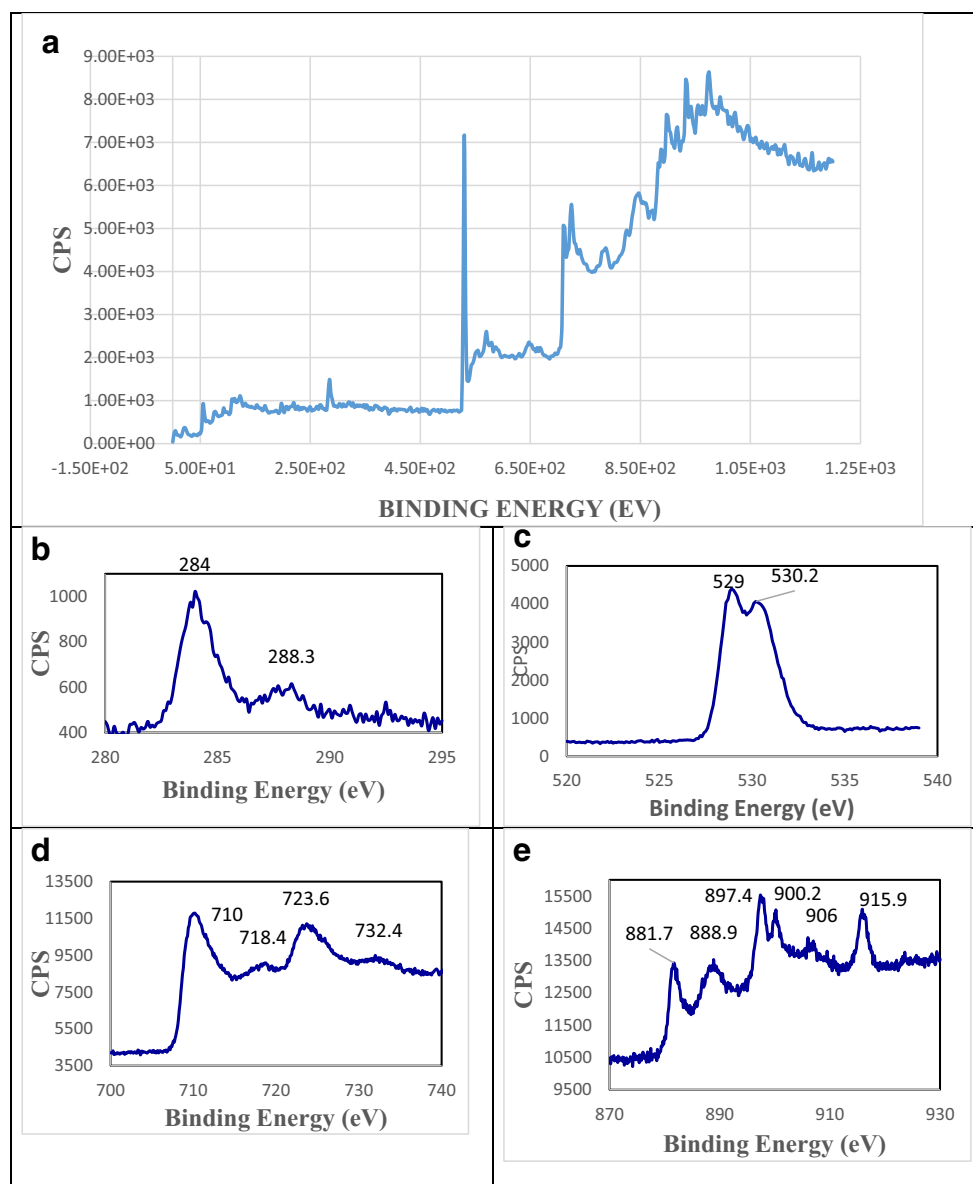
isotherm is presumably due to the presence of different types of pores in the adsorbent. The round knee-like appearance in the lower relative pressure zone resembles that of a monolayer adsorption and the low slope in the middle of isotherm indicates the first few adsorption multilayers which strongly emphasised the presence of the type I isotherm. The development of the hysteresis loop in the desorption curve ensures the presence of type IV isotherm developed due to capillary condensation in mesoporic structures present in the adsorbent.

Specific surface areas of the adsorbent before and after fluoride ion adsorption are 189.57 m^2 g^{-1} and 219.52 m^2 g^{-1}, respectively, whereas the surface area of CIHFO before surface modification with GO was 140.711 m^2 g^{-1} (Mukhopadhyay et al. 2017a, b). A notable surface area enhancement was observed after application of GO as surface modifier of CIHFO. The increase in the surface area with the decrease in pore size supports strongly the accumulation of fluoride ions within the pores of GO–CIHFO. Ionic radius of fluoride ion is much smaller than that of hydroxyl ion. Ionic exchange between F^- and OH^- is supposed to be responsible for an enormous change in the structure of the adsorbent which in turn enhances the surface area after fluoride adsorption. Pore volumes before and after fluoride ion adsorption were found to be 0.147993 $cm^3.g^{-1}$ and 0.127207 $cm^3.g^{-1}$ respectively (Fig. 6c). The decrease in pores volume also supports the adsorption of fluoride ions inside the pores of the adsorbent materials which in turn increases the surface area of the adsorbent.

Effect of varying degree of mass weight percentage of GO content in CIHFO on fluoride

To evaluate the effect on fluoride adsorption capacity after doping of GO into the surface of CIHFO, a series of batch experiments have been conducted (Fig. S6A). It was observed that with the increase of massweight percentage of GO up to

Fig. 5 XPS spectrum of the CIHFO shows **a** Full spectrum, **b** C 1 s spectrum, **c** O 1 s spectrum, **d** Fe 2p spectrum and **e** Ce 3d spectrum

Effect of pH upon fluoride adsorption capacity of GO−CIHFO

Initial solution pH and pH_{ZPC} of any adsorbent are considered two important factors that play a crucial role in any adsorption mechanism of adsorbate over adsorbent. Adsorption of any anion is influenced by the presence of hydroxyl ions in solution. To apprehend fluoride adsorption over GO−CIHFO, a set of experiments were carried out in the pH range 3–10 with adsorbent dose (0.2 g L^{-1}), temperature 303 K, and with initial fluoride concentration 5.0 and 15.0 mg L^{-1}. The pH_{ZPC} of GO–CIHFO was found to be 6.2 (± 0.2), depicting that the adsorbent surface is positive below pH_{ZPC} and negative above pH_{ZPC}. Figure 7a and b represent pictorial explanations of the effect of pH_{ZPC} of the adsorbent and also the effect of solution pH on the fluoride adsorption capacity of GO–CIHFO, respectively. It was observed from experimental results that maximum equilibrium adsorption capacity was obtained at pH 3.0 for both fluoride concentrations (22.43 mg F g^{-1} and 33 mg F g^{-1}, respectively). Moreover, the fluoride adsorption capacity GO–CIHFO reduced drastically at pH
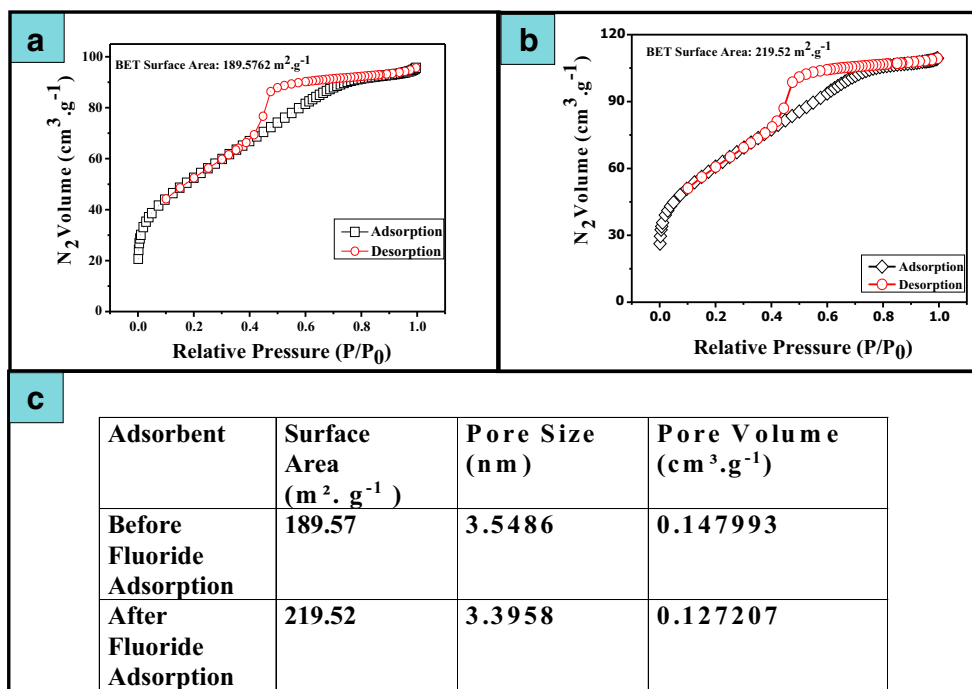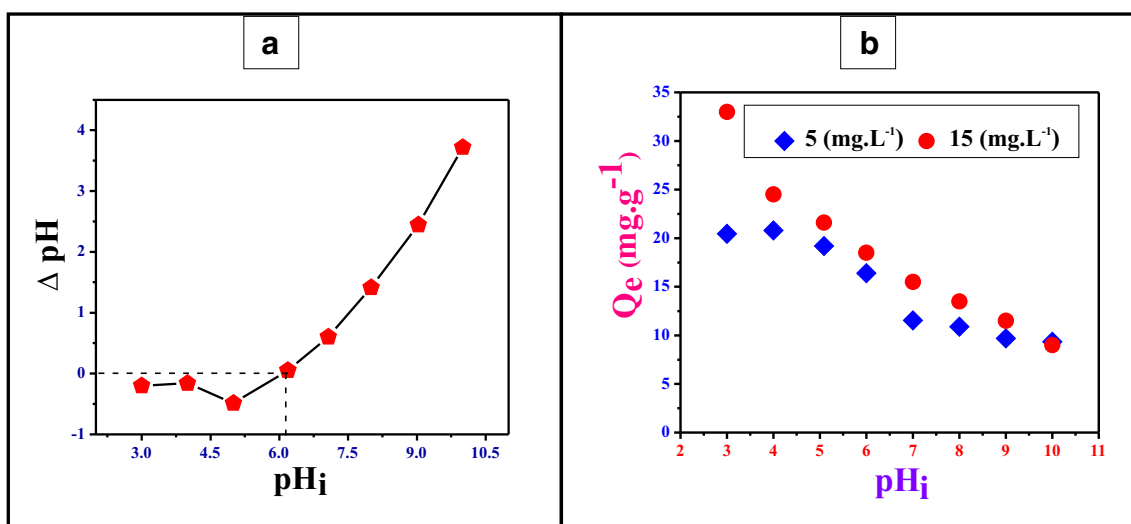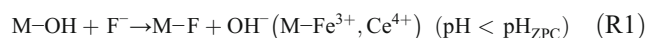
10%, the fluoride adsorption capacity of GO−CIHFO has been increased in contrast to pure mixed metal oxide. After such percentage level of GO incorporation, no such noticeable increment in fluoride adsorption capacity was observed. The main aim of this study is to develop a cost-effective material as water purifier that can be applied primarily in the fluoride-affected region of West Bengal (India) at an affordable price. To achieve this goal, 10% GO−CIHFO is selected for the rest of the experimental studies.

Fig. 6 **a**, **b** Plots of N$_2$ (vapour) (cm^3 g^{-1}) adsorbed and desorbed against relative pressure for the BET isotherm plots of GO-CIHFO before fluoride adsorption and after fluoride adsorption uponGO-CIHFO. **c** Represents details of surface area change, pore size, pore volume before and after fluoride adsorption upon GO-CIHFO

| Adsorbent	Surface Area (m^2. g^{-1})	Pore Size (nm)	Pore Volume (cm^3.g^{-1})
Before Fluoride Adsorption	189.57	3.5486	0.147993
After Fluoride Adsorption	219.52	3.3958	0.127207

> 7. Such a declining trend of fluoride uptake capacity can be justified by the fact that with increasing pH, the adsorbent retains a negative surface charge (pH > pH$_{zpc}$), which leans towards Coulombic repulsion for negatively charged fluoride ions. The concentration of hydroxyl ions (OH^{-1}) also increased at the basic pH range that also competed with the fluoride for the active binding sites of the adsorbent (Barathi et al. 2014; Mohan et al. 2016a, b; Mukhopadhyay et al. 2017a, b).

As per HSAB principle, Fe^{3+} and Ce^{4+} are act as a hard acid. Hard acids prefer binding to the hard bases to give ionic complexes. In aqueous medium, Fe^{3+} and Ce^{4+} could be present as cationic hydroxide forms and could easily interact with fluoride ions by electrostatic attraction. When solution pH is in the acidic range, adsorption occurs by electrostatic interaction.

$$M-OH + F^- \rightarrow M-F + OH^- \left(M-Fe^{3+}, Ce^{4+}\right) \ (pH < pH_{ZPC}) \quad (R1)$$


Fig. 7 **a** Plot of Δ pH versus pH$_i$ for the estimation of pH$_{ZPC}$ of the adsorbent GO-CIHFO. **b** Plots of Initial solution pH versus fluoride adsorption capacity to evaluate effect of initial pH upon fluoride adsorption over GO–CIHFO

At basic solution pH range, protonation of surface occurs. In such condition, the GO–CIHFO surface is to be negative and imparts Coulombic repulsion on fluoride ion. This can be demonstrated by R_2.

$$M-OH + F^- + OH^- \rightarrow M-O^- + F^- + OH_2 (M-Fe^{3+}, Ce^{4+})(pH > pH_{ZPC})$$
$$(R2)$$
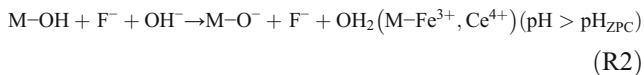
Fluoride adsorption over GO–CIHFO can be happened by ligand/anion exchange or by hydrogen bonding.

$$M-OH_2^+ + F^- \rightarrow M-F + H_2O \ (M-Fe^{3+}, Ce^{4+}) \qquad (R3)$$

$$O-H + F^- \rightarrow O-H \cdots F^- \qquad (R4)$$
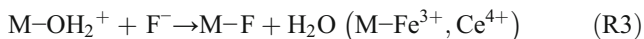
Finally, it can be concluded that fluoride adsorption over GO–CIHFO is a combination of hydrogen bonding and electrostatic interaction and also involved ligand exchange between hydroxyl groups and fluoride ions (Mohan et al. 2016a, b).

Effect of adsorbent dose

Fig. S6B reveals the dose variation plot to determine the effect of adsorbent dose on fluoride adsorption capacity (Q_e, mg F g^{-1}) with increasing dosage from 0.01 to 1.0 g NC in 50 mL of fluoride solution (C_i = 10.0 and 15.0 mg L^{-1}) for adsorption reaction at 30 °C (303 K) and at pH$_i$ ~ 7.0. It has been apparently observed from the plot that the fluoride adsorption capacity (Q_e, mg F g^{-1}) declined for a given C_i (mg L^{-1}) value with the increase of adsorbent dose. Such observation can be justified well by the surface site heterogeneity model, in which any adsorbent surface site can be visualised as being composed of a series of spectra of binding energies. At a low adsorbent dose, the entire spectrua of the sites are exposed to adsorbate molecules and surface adsorption naturally proceeds at a brusque rate resulting in greater Q_e (mg F g^{-1}) value whereas a rescindable condition will set with the rise of the adsorbent dose (Biswas et al. 2009; Saha et al. 2015; Mukhopadhyay et al. 2017a, b). A comparison of fluoride adsorption capacity of various adsorbents is reported in Table 1.

Effect of contact time on adsorption process and kinetic modelling

The effect of contact time with variation of both initial fluoride concentration and temperature upon fluoride uptake capacity of proposed adsorbent GO–CIHFO was studied sequentially to comprehend the pattern of adsorption mechanism of the ongoing adsorption process. Experiments were carried out with a fixed adsorbent dose (0.2 .L^{-1}) along with different fluoride concentrations (5 mg L^{-1}, 10 mg L^{-1}, and 15 mg L^{-1}) at temperature 303 K with two solution pH (pH 3.0 and pH 7.0). Primarily, the rate of adsorption is vastly influenced by the available free active binding sites of the proposed adsorbent and the high concentration gradient of the fluoride. It was observed that in all experimental adsorption set up, saturation time (equilibrium time) is highly independent of the initial concentration (C_i) of the fluoride solution. The fluoride uptake was found to be in a rising trend with the increase of the initial fluoride concentration (applicable for both, solution pH 3.0 and pH 7.0 respectively) until equilibrium time was achieved.

Time–rate adsorption of the proposed adsorbent, on fluoride uptake at different temperatures (288 K, 303 K, and 313 K) with fixed fluoride solution (15 mg L^{-1}) also revealed that the period of saturation remains unchanged irrespective of the rise of temperature in each adsorption study, thus is also independent of the temperature variation. Further, the highest fluoride adsorption capacity of GO–CIHFO was observed at room temperature.

In this study, various mathematical expressions of kinetic models such as pseudo-first order and pseudo-second-order kinetics models, mass transfer study, intra-particle diffusion model, Elovich model, and Richenberg model have been applied to explore the rate-controlling step and actual adsorption mechanism of fluoride by the proposed adsorbent involved in present process.

Pseudo-first order and pseudo-second-order kinetic models

Kinetic data of the present study were analysed by the most universally used non-linear form of PFO (Eq. 5) and PSO (Eq. 6) model equations. The non-linear plots of the kinetic data by PSO model and PFO model fitting are shown in Fig. 8 and Fig. S7, respectively. The parameters of the kinetic model Eqs. (5)–(6) as estimated from the plots are demonstrated in Table-S2 and Table-S3. Emphasising on the values of the regression coefficient (R^2), it can be said that the fluoride adsorption over GO–CIHFO surfaces has occurred almost in accordance with the PSO kinetic model. The $Q_{t(exp)}$ values were found too close to the modelled Q_t value from the PFO kinetic model at any particular time and temperature (applicable for both solution pH 3.0 and pH 7.0 respectively). The chemisorption is one of the controlling factors of any adsorption kinetics and is expressed by the PSO model. Hence, it can be assumed from such results that as the fluoride adsorption process was well fitted with the PSO model, then the adsorption process might be following chemisorptions (Biswas et al. 2009; Mohan et al. 2016a, b; Mukhopadhyay et al. 2017a, b).

Mass transfer study

The Fig. S8 represents the Mckay et al. (1981) model plot for the mass transfer of fluoride in both solution pH 3.0 and pH 7.0 respectively (McKay et al. 1981). The plot of good linear

Table 1 Comparison of GO incorporated CIHFO nanocomposite with previously reported adsorbents for the removal of fluoride in terms of uptake capacity

S No.	Adsorbent	Adsorption Capacity		pH	Fluoride concentration (mg L^{-1})	Adsorbent dose (g L^{-1})	Reference
		Langmuir Q_m (mg g^{-1})	Freundlich K_F (mg g^{-1})				
1.	Ce–Fe bimetal oxides	60.97	21.99	7.0	–	0.5	(Tang and Zhang 2016)
2.	Ce (IV)+Zr (IV) mixed oxide	19.5	8.566	5.8 (±2)	5.0–35.0	0.05 g in 50 mL solution	(Ghosh et al. 2014)
3.	Iron (III)–tin (IV) bimetal mixed oxide	10.47	1.15	6.4 (± 2)	10.0–50.0	0.10 g in 50 mL solution	(Biswas et al. 2009)
4.	Al–Ce hybrid oxide	91.4	–	6.0	2.0 to 15.0	0.01 g in 100 mL solution	(Liu et al. 2010)
5.	Mn–Ce oxide	137.5	–	6.0	6 equilibrium concentration	0.01 g in 100 mL solution	(Deng et al. 2011)
6.	CZ–CAB	158.7	4.95	7.0	2–200	0.5	(Chen et al. 2016a)
7.	Ce oxide	25.3	–	7.0	15	0.05 g in 100 mL solution	(Mukhopadhyay et al. 2017a, b)
8.	(LDH-n-MABs)	61.8	1.114	5.0	2.0–70.0	0.5	(Gao et al. 2014)
9.	Graphene	35.59	2.49	7.0	5.0–40.0	0.5	(Li et al. 2011)
10.	FeOOH+Ac/GO	19.82	5.5412	2.7–10.39	10–150	50 mg in 20 mL solution	(Kuang et al. 2017)
11.	FeOOH/GO	17.65	5.508	2.11–10.39	10–150	50 mg in 20 mL solution	(Kuang et al. 2017)
12.	rGO/ZrO$_2$	46		7.0	25	0.5	(Mohan et al. 2016a)
13.	Al-O-(OH)-incorporated graphene oxide	51.41	17.18	7.5	5.0–60.0	0.05 g. 0.1 L^{-1}	(Zhang et al. 2015)
14.	HIAGO**	27.75	8.032	7.0	–	–	(Kanrar et al. 2016)
15.	Aluminium oxide hydroxide (nano-AlOOH)	62.5	20.75	7.0	5-30	1.6	(Adeno et al. 2014)
16.	CIHFO*	32.62	8.58	7.0	10.0–60.0	0.05 g in 100 mL solution	(Mukhopadhyay et al. 2017a, b)
17.	GO	1.43	0.26	7.0	30	1 g in 2 L	(Li et al. 2013)
18.	GO-incorporated CIHFO	190.61 136.24		3.0 and 7.0	5.0–60.0	0.2	Present work

*Cerium(IV)-incorporated hydrous iron(III) oxide; **Graphene oxide-incorporated iron–aluminium mixed oxide

fitting with the experimental data denoted that the external mass transfer step was present during the adsorption process. The mass transfer coefficients (β_1) for the diffusion of fluoride from the liquid film boundary to the surface of GO–CIHFO have been determined by the slopes of the plots of ln [C_t/C_i − 1/(1 + mk)] vs. t (min) at different temperature (288 K, 303K, and 313 K) with fixed fluoride concentration (15 mg.L^{-1}) with both solution pH 3.0 and pH 7.0, respectively, and are shown in Fig. S8 and values are given in Table-S3. All the values of mass transfer coefficient act as an indication of sufficiently rapid transfer of adsorbate species from bulk solution to the surface or interface for both the solution pH.

Intra-particle diffusion model

The plot of Q_t vs. $t^{0.5}$ (min) shown in Fig. S9-12(A-C) signifies the corresponding Weber–Morris model to evaluate the

prospect of IPD on the adsorption process of fluoride onto GO–CIHFO (Weber and Morris). The plots were found to be significantly linear with high value of R^2, and K_{id} values have been determined by their respective slopes at varied experimental conditions (Table-S2 and Table-S3). If the plot of Q_t vs. $t^{0.5}$ is a straight line and passes through the origin, then the IPD is thought to be as the RDS (Biswas et al. 2009; Ranjan et al. 2009).In this adsorption system, although these plots are linear, they did not pass through the origin, which indicated that the IPD was not the sole RDS. Hence, it can be assumed that fluoride adsorption over the proposed adsorbent occurred via a complex mechanism involving both the external mass transfer and the IPD as the RDS. This observation was further strengthened by the value of the IPD coefficient (D), which can be calculated by Eq. 9.

Here, r (cm) represents the average radius of the adsorbent particle and $t^{0.5}$ (min) is the time required for half of the
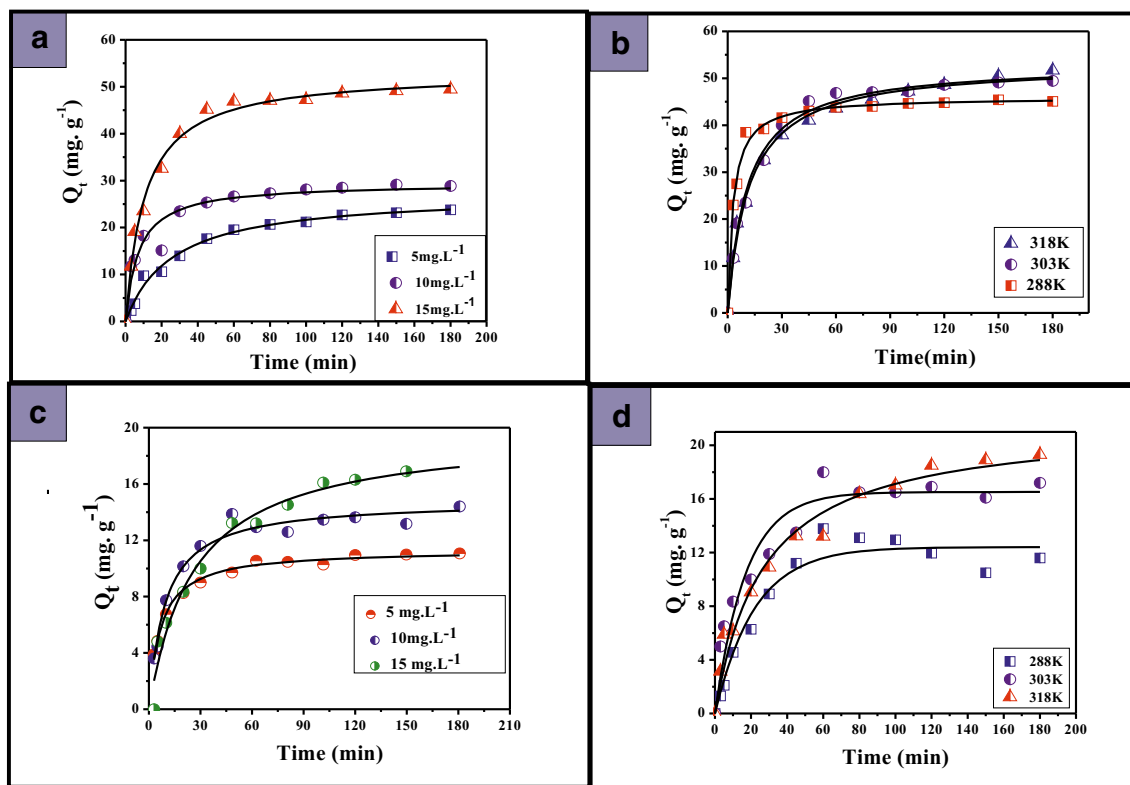
Fig. 8 **a**, **b** The plots of fluoride adsorption capacity at any time, Q_t (mg g^{-1}) versus time, t (min) including non-linear pseudo second order (—) at three different concentrations (5 mg.L^{-1}, 10 mg L^{-1} and 15 mg L^{-1}) at temperature 303 K (ionic strength = 1 M) and pH 3.0 and pH 7.0 respectively. **b**, **d** The plots of fluoride adsorption capacity at any time, Q$_t$ (mg g^{-1}) versus time, t (min) including non-linear pseudo second order (—) at three temperature (288 K, 303 K and 313 K) respectively with active fluoride concentration 15 mg L^{-1} (ionic strength = 1 M) at pH 3.0 and pH 7.0 respectively

adsorption. If the D value is in the range of 10^{-11} (cm^2 s^{-1}) then IPD is the only rate-determining step. In the present adsorption system, the value of D obtained as (7.46×10^{-8} cm^2 s^{-1}) was in the order of 10^{-8}, designating that IPD was not the only RDS (Mohan et al. 2016a, b).

Elovich model

Elovich model (Novoselov 2004) is another widely accepted kinetic model used successfully to describe second-order kinetics with a postulation that the solid surface of the adsorbent is energetically heterogeneous. It has been broadly accepted that chemisorption process can be elucidated by its linear form of semi-empirical equation (Eq. 10). The Elovich coefficients have been assumed Fig. S9-12(D-F) from the plots Q_t vs. ln (t) (min). The initial adsorption rate, a, and desorption constant, b, were calculated from the slope and the intercept of the straight line plots and values obtained from plots have been tabularized in Table-S2 and Table-S3. It has been observed that the applicability of the simple Elovich equation for the present kinetic data indicates that the Elovich equation was able to describe properly the kinetics of fluoride adsorption on GO–CIHFO. In acidic solution (pH 3.0) as well as in neutral solution pH, the value of a and b varied as a function of both

solution concentration and solution temperature. Good correlation coefficient (R^2) for both concentration variation and temperature variation implied that adsorption kinetics followed by the pseudo-second-order kinetic model is based on the assumption that chemisorption may be the rate-determining step involving ion exchange between adsorbent and adsorbate (Ranjan et al. 2009).

Reichenberg model

Fig. S10 & S12 (G-I) present the plots of the Reichenberg model (Reichenberg 1953) [β_t vs. t (min)] at different solution concentrations (5.0, 10.0, and 15.0 mg L^{-1}) at temperature 303 K and at different temperature (288 K, 303K and 313 K) in neutral pH. Whereas Fig. S9 & S11(G-I) denote the plots of the Richenberg model [β_t vs. t (min)] with solution concentration (5 mg. L^{-1}, 10 mg. L^{-1}, and 15 mg. L^{-1}) at temperature 303 K and different temperatures (288 K, 303K, and 313 K) in acidic pH.

The plots with good linearity were accompanied with high correlation coefficient (R^2) values (given in Table-S2 and Table-S3) and did not pass through the origin. These results is indicative of the fact that IPD is not the only RDS and this also supports the results obtained from IPD model.

The factor β_t was calculated from the slope and used to calculate the effective D_i and both are recorded in Table-S2 and Table-S3. If the values of D_i have been ranged between 10^{-6} and 10^{-8} cm^2 s^{-1}, the RDS dominated the external mass transfer, whereas the values of D_i when obtained in the range of 10^{-11} to 10^{-13} cm^2 s^{-1}, IPD is considered the rate-controlling step. From Table-S2 and Table-S3, it has been observed that the values of D_i for the adsorption of fluoride on the GO–CIHFO was in the order of 10^{-6} cm^2 s^{-1}, which is more than 10^{-11} cm^2 s^{-1}; then, IPD was not the only rate-controlling step; external mass transfer was also involved in the adsorption process. Values of film diffusion (D_1) and pore diffusion (D_2) were assessed and mentioned in Table-S2 and Table-S3. Negative exponential values with the same order of magnitude assure that both film and pore diffusion processes were involved in adsorption mechanism (Hamayun et al. 2014).

Equilibrium analysis

To recognise the adsorption feasibility of a newly developed adsorbent, different adsorption isotherm models were applied for better understanding of the adsorption process. Langmuir and Freundlich and D–R isotherms are the most convenient fundamental isotherm models that can be applied to illustrate the surface properties and adsorption mechanism. For the adsorption isotherm study, experiments were carried out at four different temperatures (288, 303, 313, and 323 K) using a thermostatic shaker with an initial fluoride concentration in a range of 5 to 60 mg L^{-1}, by varying solution pH 3.0 and pH 7.0 and with an adsorbent dose 0.2 g L^{-1}.

Langmuir isotherm

The Langmuir isotherm constants, Q_m (the maximum mono-layer adsorption capacity, mg F. $^{-1}$) and K_L (the equilibrium constant related to the net enthalpy change of the reaction, L mg^{-1}) were obtained from the plot of non-linear form of Langmuir equation (Eq. 17) with the help of the Origin software spreadsheet presented in Table 2 and in Figs. 9 and 10. The Langmuir uptake capacity of GO–CIHFO was found 115.6 mg F g^{-1} at pH 3.0 and 80.42 mg F g^{-1} at pH 7.0 at 303 K (30 °C). The increasing trend of the Q_m value with higher temperature range (applicable for both solution pH 3.0 and pH 7.0) indicated the endothermic nature of the adsorption process (Biswas et al. 2009; Ghosh et al. 2014; Mohan et al. 2016a, b).

Freundlich isotherm

The values of regression coefficient (R^2) and Freundlich constant (n and K_F) obtained from the non-linear Freundlich isotherm equation (H. M. F. Freundlich 1906) (Eq. 18) analysis are given in Table 2 and in Figs. 9 and 10. Based on values of regression coefficient (R^2), it can be easily concluded that the fitting of equilibrium data was much better with the Freundlich model rather than with the Langmuir model. From the assessed values of n, it was perceived that the degree of Freundlich coefficient ($1/n$) is laid between 0 and 1 that assures a favourable adsorption of fluoride upon GO–CIHFO. The highest values of K_F (Freundlich adsorption capacity) was obtained at temperature 303 K for solution pH 3.0 and at

Table 2 Isotherm parameters of fluoride adsorption reactions with GO incorporated CIHFO at pH 3.0 (±0.2) and pH 7.0(±0.2) at 288, 303, 313 and 323 K

Isotherm Model	Parameters	pH 3.0				pH 7.0			
		Temperature (K)				Temperature (K)			
		288	303	313	323	288	303	313	323
Langmuir	Q_m (mg g^{-1})	89.4	115.6	142.78	190.61	56.02	80.42	97.02	136.24
	K_L (L mg^{-1})	0.08	0.086	0.067	0.024	0.093	0.027	0.022	0.015
	R^2	0.96	0.95	0.98	0.95	0.95	0.97	0.98	0.97
Freundlich	n	2.33	2.28	1.97	1.55	2.55	1.69	1.58	1.40
	$1/n$	0.42	0.43	0.5	0.64	0.39	0.59	0.63	0.71
	K_F (mg g^{-1})	14.4	18.41	17.05	8.84	10.38	4.71	4.75	3.81
	R^2	0.99	0.97	0.99	0.97	0.95	0.98	0.97	0.99
Dubinin–Radushkevich	Q_m (mol kg^{-1})	11.3	14.05	20.21	17.28	7.158	9.02	16.60	19.01
	β (mol^2 kJ^{-1}) × 10^{-3}	-5.17	-4.51	-4.98	-4.90	-5.13	-5.99	-7.22	-7.06
	E_{DR} (kJ mol^{-1})	9.83	10.52	10.02	10.10	9.87	9.13	8.32	8.41
	R^2	0.99	0.96	0.97	0.92	0.97	0.93	0.99	0.97
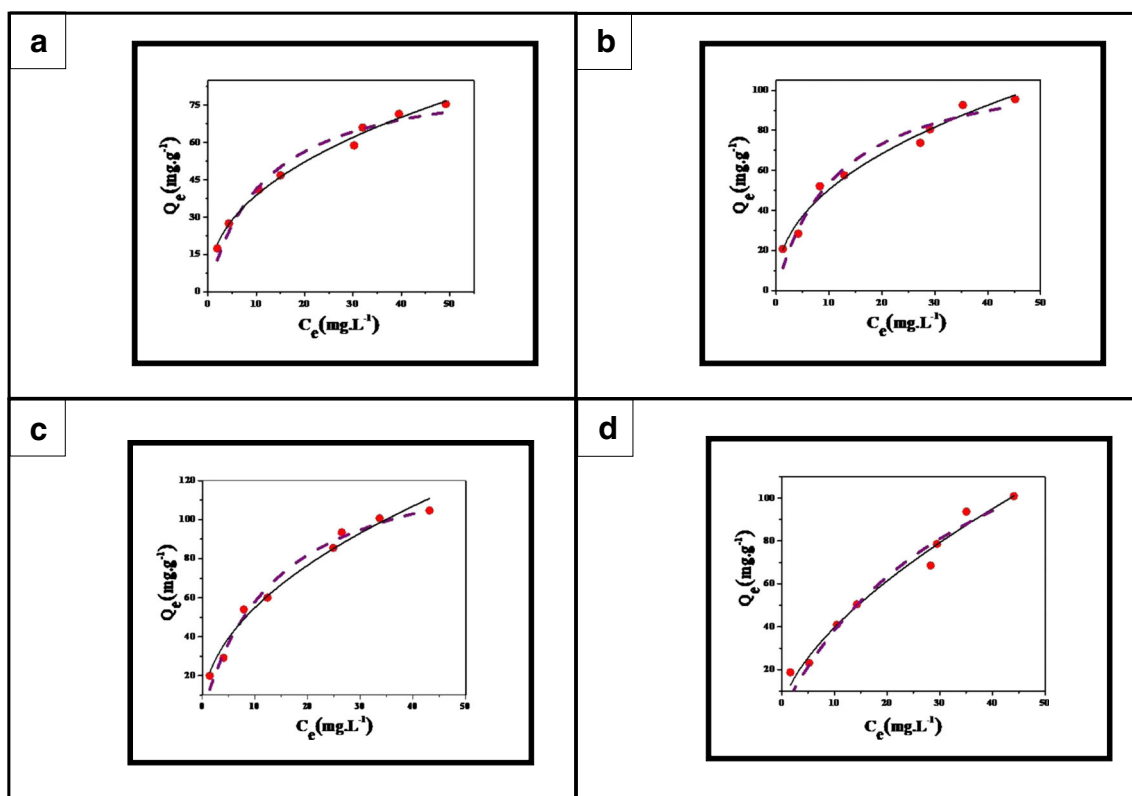
Fig. 9 **a–d** Plots of equilibrium adsorption capacity (Q_e) versus equilibrium concentration (C_e) of fluoride and nonlinear fitting of data with Langmuir and Freundlich models for adsorption of fluoride on adsorbent at pH 3.0 with four different temperatures 288 K, 303 K, 313 K, and 323 K respectively

temperature 288 K for solution pH 7.0. Henceforth, there was no such brisk enhancement in K_F (Freundlich adsorption capacity) values in higher temperature zone in neutral pH. Therefore, 303 K and solution pH 7.0 can be considered optimised temperature and pH, respectively, for adsorption of fluoride on GO–CIHFO (Mohan et al. 2016a, b).

D–R isotherm

Evaluation of the free energy of reaction of any adsorption process and to envisage the nature of adsorption, whether physical, ion-exchange, or chemical, the D–R isotherm is the most widely accepted model in this field (Dubinin and Radushkevich 1947). To obtain D–R isotherm parameters, $\ln Q_e$ vs. E^2 were plotted and found to be significantly linear at all the temperatures (Fig. S13 & Fig. S14).The parameters of this isotherm, such as energy of adsorption E_{DR} (kJ mol^{-1}), β (mol^2 kJ^{-2}), and R^2, are mentioned in Table 2. The substantially high value of R^2 associated with applied temperatures suggested the applicability of the D–R isotherm. With the D–R equation and according to the value of E_{DR}, an adsorption process can be categorised into three types such as (i) physisorption if $E_{DR} = 8.0$ kJ mol^{-1}, (ii) ion-exchange if $E_{DR} = 8.0$–16.0 kJ mol^{-1}, and (iii)

chemisorption if $E_{DR} > 16.0$ kJ mol^{-1} (Ghosh et al. 2014; Mukhopadhyay et al. 2017a, b). E_{DR} values established from the D–R isotherm were ranged between 9.83 and 10.52 when fluoride solution pH was 3.0 and 8.32–9.87 with fluoride solution pH was 7.0, indicating the adsorption of fluoride occurring mostly via ion-exchange phenomena when solution pH 3.0 but neutral pH adsorption of fluoride show the predominant trait of physisorption inclined to ion-exchange phenomena. At 303 K temperature, the E_{DR} obtained for the present case is 10.52 kJ mol^{-1} (solution pH 3.0) and 9.13 kJ mol^{-1} (solution pH 7.0) strongly emphasised on the ion-exchange phenomenon.

Thermodynamics studies

The plot of $\ln K_C$ vs. $1/T$ (Van't Hoff plot) for fluoride adsorption for both solution pH 3.0 and pH 7.0 is shown in Fig. S14.The thermodynamic parameters ($\Delta G°$, $\Delta H°$, $\Delta S°$) thus calculated are updated in Table-S4. The negative values of $\Delta G°$ (for both solution pH 3.0 and pH 7.0) specified the spontaneous nature of the adsorption process. Hence, adsorptive forces required for the reaction are fairly strong enough to overcome the potential barrier and greater negative values of $\Delta G°$ associated with rise of temperature indicated that higher
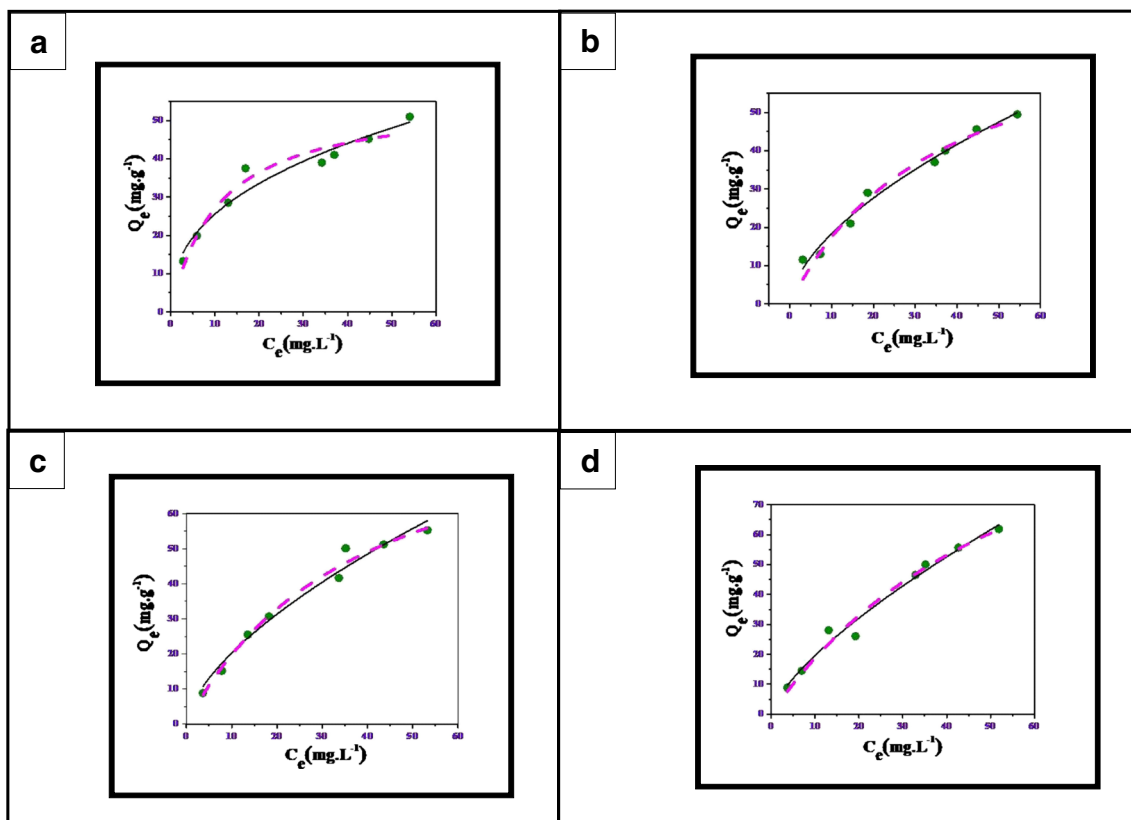
Fig. 10 **a–d** Plots of equilibrium adsorption capacity (Q_e) versus equilibrium concentration (C_e) of fluoride and nonlinear fitting of data with Langmuir and Freundlich models for adsorption of fluoride on adsorbent at pH 7.0 with four different temperatures 288 K, 303 K, 313 K, and 323 K respectively

temperature favours the adsorption process. Negative values of enthalpy ($\Delta H°$) in both solution pH values suggested the endothermic nature of the adsorption process. The positive values of $\Delta S°$ for both conditions of the whole adsorption experiment system recommended a high degree of freedom of solute molecules owing to adsorption; thus, randomness was increased during the adsorption process. This was presumably due to the desorption process that simultaneously took place during adsorption, increasing the entropy ($\Delta S°$) at the solid–liquid interface (Hamayun et al. 2014; Saha et al. 2015; Mukhopadhyay et al. 2017a, b).

Activation energy

Activation energy of any kind of reaction and can be expressed by Arrhenius equation and can be expressed as

$$k_2 = A \exp(-E_a/RT) \tag{22}$$

Here, k_2 is the rate constant of pseudo-second-order kinetic model (g mg^{-1} min^{-1}), A (g mg^{-1} min^{-1}) is a temperature independent factor, and E_a (KJ mol^{-1}) is the activation energy of any particular reaction. R and T are well known and

mentioned earlier. The logarithm of the above equation can be demonstrated by a linear relationship of the Arrhenius equation and can be represented as below.

$$\ln k_2 = \ln A + (-E_a/R)1/T \tag{23}$$

The plot of $\ln k_2$ against $1/T$, a straight line with slope ($-E_a/R$) was obtained and presented in Fig. S15. The magnitude of activation energy (E_a) for adsorption of fluoride on the surface of GO–CIHFO has been evaluated from slope of the plot was 44.47 KJ mol^{-1} and 22.61 KJ mol^{-1} respectively for the solution pH 3.0 and pH 7.0. The magnitude of E_a is lesser than 42 KJ mol^{-1}; then, the diffusion control process is thought to be accompanying the adsorption process and the E_a value higher than 42 KJ mol^{-1} is envisaged and a chemically controlled reaction process also occurred. Here, the high magnitude of activation energy for this adsorption study implies that fluoride has a high combining affinity with the proposed adsorbent surface as the diffusion process prefers the movement of the solute to the external surface of the adsorbent. Considering the value of E_a, it can be assumed fluoride adsorption upon the surface of proposed material is supposed to be associated with ion exchange with slight inclining trend to chemisorption when solution pH 3.0 that also significantly supports the

adsorption pattern obtained from the D–R isotherm study (Podder and Majumder 2016).

Effect of co-occurring ions on fluoride adsorption

Groundwater resource contains a wide range of anions such as SO_4^{2-}, HCO_3^- and HPO_4^{2-} in addition with F^- which may have affinity towards the same active sites on adsorbent as reported earlier (Ghosh et al. 2014; Barathi et al. 2014; Mukhopadhyay et al. 2017a, b). A series of experiments were carried out in the presence of these anions with different concentrations along with a blank sample to explore their influence upon fluoride uptake capacity. In the blank sample, fluoride adsorption capacity has been obtained 13.9 mg F g^{-1}. It was observed that these anions at altered concentrations impose no such adverse effects upon the fluoride adsorption capacity of GO–CIHFO even at the high concentration pictorially presented in Fig. S16. It presumably occurs due to weak or lack of interaction between adsorbent active sites and the said anions.

Desorption and re-usability of the proposed adsorbent

Regeneration is a useful tool to regain the adsorptive capacity of any adsorbent. Development of a cost-effective adsorbent and commercialisation of the material is highly dependent on the recycling nature of the adsorbent. Desorption study is considered an efficient process to evaluate the recycling and re-usability of any adsorbent. The fluoride-free material is then air dried and collected to repeat the aforesaid adsorption-desorption study (Barathi et al. 2014; Mohan et al. 2016a, b). The adsorbents were reused for five cycles in this study. Fig. S15C depicted that no such rise in fluoride concentration was noticed in solution up to pH 9.0; afterward, desorption efficiency of fluoride sequentially increased to 73.77 % at pH 13.0. During recycling, the percentage of adsorption of fluoride was found to be 69.19% and 16.66% respectively for the 1st and 5th cycles of reuse (Fig. S15D).

Removal of fluoride from a natural groundwater sample

Purulia District situated in the eastern fringe of the State of West Bengal, India, is now in the limelight for the high concentration of fluoride in groundwater and the situation is getting worse day after day. Considering such adverse situation of this region, water samples have been collected from few selective hand pump-attached tube wells of Kashipur block of Raghunathpur Subdivision of Purulia District (Fig. S17). Water sample collected from (Latitude—23° 28′ 303″ N;

Longitude—86° 40′ 027″ E, elevation—161 m) Kharai village of Kashipur block of Purulia district, West Bengal, was reported with high fluoride concentration (9.05 mg L^{-1}), among all collected samples ('File.kml here'). Some physicchemical parameters such as pH (7.36), iron (total) (0.77 mg.L^{-1}), calcium (18.05 mg L^{-1}), magnesium (3.69 mg L^{-1}), hardness (21.74 mg L^{-1}), TDS (679 mg L^{-1}), salinity (473 mg L^{-1}), conductivity (959 μS), and turbidity (18 NTU)were also carried out to evaluate overall water quality. One litre of this water sample was stirred (500 rpm) with the help of magnetic stirrer for 2 h with changing GO–CIHFO dosage from 0.1 to 1.5 g. After completion of the experiment time, treated water was filtered and analysed for the fluoride level. It was found that fluoride level reduced from 9.05 mg L^{-1} to below 1.0 mg L^{-1} when the dosage of GO–CIHFO employed was 1.2 g.L^{-1}. Thus, it can be experimentally approved that 1.2 g of GO–CIHFO can efficiently reduce fluoride level to desired concentration (1.0 mg L^{-1}) which is well below the WHO recommended guide line for maximum fluoride concentration level.

Mechanism of fluoride adsorption over GO–CIHFO

Probable mechanism of fluoride adsorption over GO–CIHFO has been assumed based on data obtained from pH effect and FTIR spectrum analysis and explained schematically presented in Scheme.1. Results of measured pH_{ZPC} and pH effect upon fluoride adsorption suggested that as per HSAB principle, in the prepared adsorbent, Fe^{3+} and Ce^{4+} are prevailing as hard acids and can easily form ionic complexes with fluoride ions by electrostatic attraction. To ascertain insight on mechanism, FTIR spectra of the fluoride-enriched adsorbent were analysed and compared with those of the unabsorbed material. Crucial shifting of peak intensity has been observed after fluoride adsorption. Shifting of bands from 3417.13 to 3243.04 cm^{-1} and from 1633.59 to 1625.88 cm^{-1} ensures the interaction between fluoride ions with surface hydroxyl groups of the adsorbent. Partial disappearance of epoxy C–O and alkoxy C–O stretching vibration band peaks in fluoride-rich adsorbent confirms chemical interaction of fluoride with these surface active sites of adsorbent. The E_{DR} value obtained at room temperature is 10.52 kJ mol^{-1} for solution pH 3.0 and 9.13 kJ mol^{-1} for solution pH 7.0 and predict that the adsorption process is predominantly ion exchange in nature. Greater negative value of ΔH^0 and moderate tendency of fluoride desorption and the magnitude of activation energy (E_a—44.47 KJ mol^{-1} and 22.61 KJ mol^{-1} for the solution pH 3.0 and pH 7.0, respectively) support the said observation.
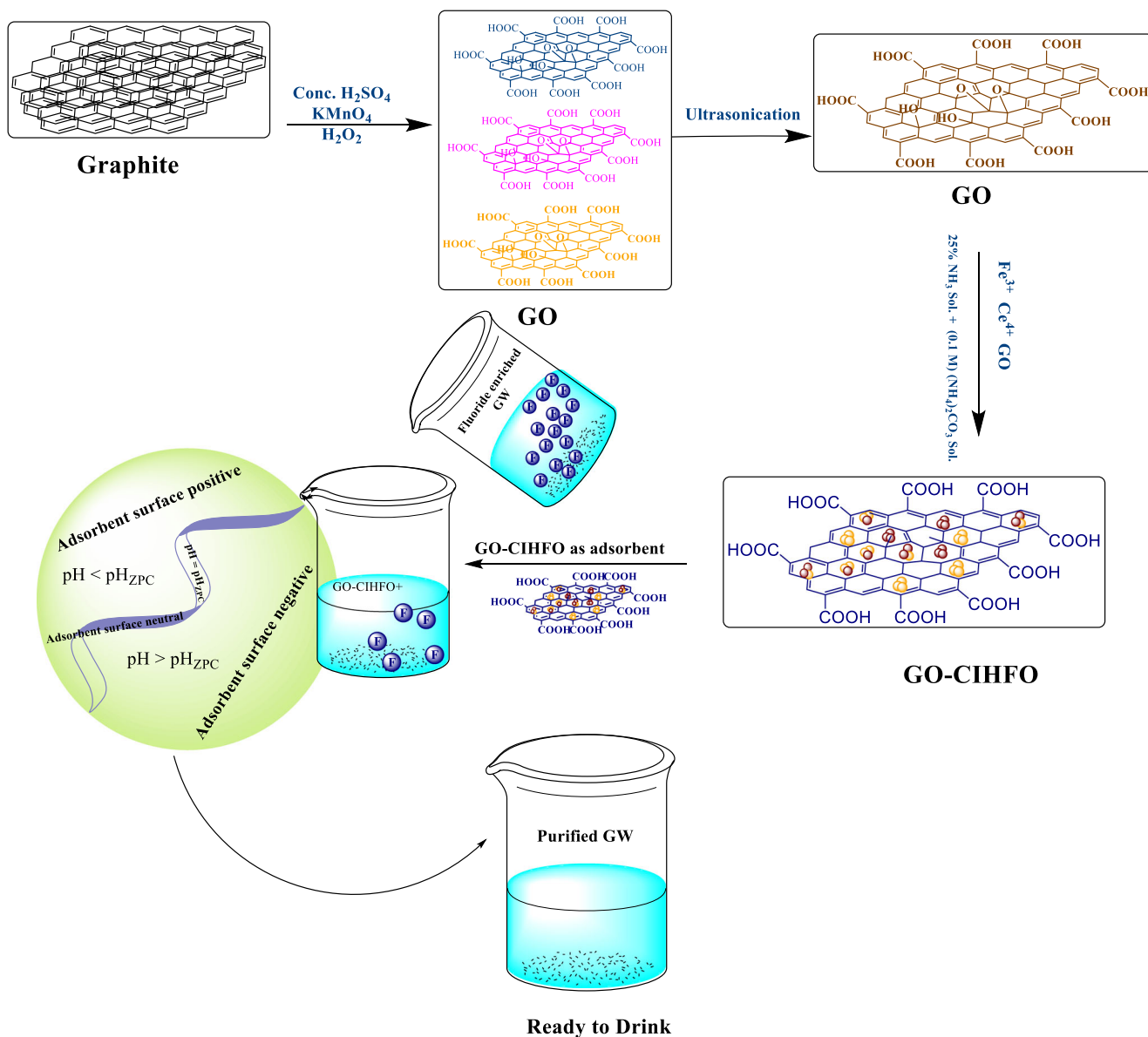
Scheme 1 Schematic presentation of proposed reactions mechanism of fluoride adsorption process involved over GO–CIHFO

Conclusion

This experimental documentation has described well the interaction between fluoride and GO–CIHFO in a wide range of pH. Surface reaction suited well to the pseudo-second-order kinetics; in addition, boundary layer (film) diffusion and external mass transfer also involved in adsorption reaction. Best fitting of isotherm data with the Freundlich isotherm model ensured multilayer adsorption had taken place during the adsorption process. Obtained Langmuir adsorption capacity for fluoride of this novel adsorbent (GO–CIHFO) is considered for evaluation of adsorptive capability of as-prepared adsorbent GO–CIHFO (190.61 mg F g^{-1}and 136.24 mg F g^{-1}for solution pH 3.0 and pH 7.0 respectively) as it was found noticeably higher than individual pure GO (3.0 mg F.g^{-1})

and CIHFO (32.62 mgF.g^{-1}) for ensuring accomplishment of the primary aim of application of GO as surface modifier over CIHFO has been achieved.

In acidic pH, entropy ($\Delta S°$) value is greater than 80 kJ mol^{-1} but in neutral pH range lower than 80 kJ mol^{-1}. It recommended that borderline chemisorption might occur at acidic pH, but in neutral pH, the adsorption process happened mostly by ion exchange. Calculated E_{DR} value and magnitude of activation energy also favoured these results. No such adverse effect of interfering ions upon fluoride adsorption occurred. It was observed that a minute amount of GO–CIHFO can treat high fluoride-containing (9.05 mg L^{-1}) groundwater and reduce the contamination level below the permissible level successfully. Application of the proposed material in a vast pH range not only suggests its usability for groundwater

treatment but also its usability as a purifier medium for fluoride-enriched industrial effluent.

References

Adeno F, Mulugeta E, Zewge F, Chebude Y (2014) Adsorptive removal of fluoride from water using nanoscale aluminium oxide hydroxide (AlOOH). Bull Chem Soc Ethiop 28:215–227. https://doi.org/10.4314/bcse.v28i2.6

Alagumuthu G, Rajan M (2008) Monitoring of fluoride concentration in ground water of Kadayam block of Tirunelveli district, India. Rasayan J Chem 1:920–928

Baltrusaitis J, Cwiertny DM, Grassian VH (2007) Adsorption of sulfur dioxide on hematite and goethite particle surfaces. Phys Chem Chem Phys 9:5542–5554. https://doi.org/10.1039/b709167b

Banerjee S, Chattopadhyaya MC (2017) Adsorption characteristics for the removal of a toxic dye, tartrazine from aqueous solutions by a low cost agricultural by-product. Arab J Chem 10:S1629–S1638.- https://doi.org/10.1016/j.arabjc.2013.06.005

Barathi M, Santhana Krishna Kumar A, Rajesh N (2013) Efficacy of novel Al–Zr impregnated cellulose adsorbent prepared using microwave irradiation for the facile defluoridation of water. J Environ Chem Eng 1:1325–1335. https://doi.org/10.1016/j.jece.2013.09.026

Barathi M, Krishna Kumar AS, Kumar CU, Rajesh N (2014) Graphene oxide–aluminium oxyhydroxide interaction and its application for the effective adsorption of fluoride. RSC Adv 4:53711–53721. https://doi.org/10.1039/C4RA10006A

Basu T, Ghosh UC (2013) Nano-structured iron(III)–cerium(IV) mixed oxide: Synthesis, characterization and arsenic sorption kinetics in the presence of co-existing ions aiming to apply for high arsenic groundwater treatment. Appl Surf Sci 283:471–481. https://doi.org/10.1016/j.apsusc.2013.06.132

Bhatnagar A, Kumar E, Sillanpää M (2011) Fluoride removal from water by adsorption—A review. Chem Eng J 171:811–840. https://doi.org/10.1016/j.cej.2011.05.028

Biswas K, Gupta K, Ghosh UC (2009) Adsorption of fluoride by hydrous iron(III)–tin(IV) bimetal mixed oxide from the aqueous solutions. Chem Eng J 149:196–206. https://doi.org/10.1016/j.cej.2008.09.047

Biswas K, Gupta K, Goswami A, Ghosh UC (2010) Fluoride removal efficiency from aqueous solution by synthetic iron(III)–aluminum(III)–chromium(III) ternary mixed oxide. Desalination 255:44–51. https://doi.org/10.1016/j.desal.2010.01.019

Briggs D (ed) (1978) Handbook of x-ray and ultraviolet photoelectron spectroscopy. Heyden, London [usw.], Rheine

Chakrabarti S, Bhattacharya HN (2013) Inferring the hydro-geochemistry of fluoride contamination in Bankura district, West Bengal: A case study. J Geol Soc India 82:379–391. https://doi.org/10.1007/s12594-013-0165-9

Chen L, He B-Y, He S, Wang TJ, Su CL, Jin Y (2012) Fe—Ti oxide nano-adsorbent synthesized by co-precipitation for fluoride removal from drinking water and its adsorption mechanism. Powder Technol 227:3–8. https://doi.org/10.1016/j.powtec.2011.11.030

Chen L, Zhang K, He J, Cai XG, Xu W, Liu JH (2016a) Performance and mechanism of hierarchically porous Ce–Zr oxide nanospheres encapsulated calcium alginate beads for fluoride removal from water. RSC Adv 6:36296–36306. https://doi.org/10.1039/C6RA01337F

Chen P, Zhang W, Li M, Ai P, Tian L, Jiang H (2016b) Facile synthesis of magnetic La–Zr composite as high effective adsorbent for fluoride removal. RSC Adv 6:35859–35867. https://doi.org/10.1039/C5RA27929A

Deng S, Liu H, Zhou W, Huang J, Yu G (2011) Mn–Ce oxide as a high-capacity adsorbent for fluoride removal from water. J Hazard Mater 186:1360–1366. https://doi.org/10.1016/j.jhazmat.2010.12.024

Drewniak S, Muzyka R, Stolarczyk A, Pustelny T, Kotyczka-Morańska M, Setkiewicz M (2016) Studies of reduced graphene oxide and graphite oxide in the aspect of their possible application in gas sensors. Sensors 16:103. https://doi.org/10.3390/s16010103

Dubinin MM, Radushkevich LV (1947) The Equation of the Characteristic Curve of Activated Charcoal. Proc Acad Sci USSR Phys Chem Sect 55:331–337

Freundlich HMF (1906) Over the Adsorption in Solution. Z Phys Chem 57:385–470

Gao C, Yu X-Y, Luo T, Jia Y, Sun B, Liu JH, Huang XJ (2014) Millimeter-sized Mg–Al-LDH nanoflake impregnated magnetic alginate beads (LDH-n-MABs): a novel bio-based sorbent for the removal of fluoride in water. J Mater Chem A 2:2119–2128. https://doi.org/10.1039/C3TA13526H

Ghosh A, Chakrabarti S, Biswas K, Ghosh UC (2014) Agglomerated nanoparticles of hydrous Ce(IV)+Zr(IV) mixed oxide: preparation, characterization and physicochemical aspects on fluoride adsorption. Appl Surf Sci 307:665–676. https://doi.org/10.1016/j.apsusc.2014.04.095

Hamayun M, Mahmood T, Naeem A et al (2014) Equilibrium and kinetics studies of arsenate adsorption by FePO. Chemosphere 99:207–215. https://doi.org/10.1016/j.chemosphere.2013.10.075

Hummers WS, Offeman RE (1958) Preparation of graphitic oxide. J Am Chem Soc 80:1339–1339. https://doi.org/10.1021/ja01539a017

Jagtap S, Yenkie MK, Labhsetwar N, Rayalu S (2012) Fluoride in drinking water and defluoridation of water. Chem Rev 112:2454–2466. https://doi.org/10.1021/cr2002855

Kanrar S, Debnath S, De P et al (2016) Preparation, characterization and evaluation of fluoride adsorption efficiency from water of iron-aluminium oxide-graphene oxide composite material. Chem Eng J 306:269–279. https://doi.org/10.1016/j.cej.2016.07.037

Kuang L, Liu Y, Fu D, Zhao Y (2017) FeOOH-graphene oxide nanocomposites for fluoride removal from water: Acetate mediated nano FeOOH growth and adsorption mechanism. J Colloid Interface Sci 490:259–269. https://doi.org/10.1016/j.jcis.2016.11.071

Langevoort JC, Sutherland I, Hanekamp LJ, Gellings PJ (1987) On the oxide formation on stainless steels AISI 304 and incoloy 800H investigated with XPS. Appl Surf Sci 28:167–179. https://doi.org/10.1016/0169-4332(87)90062-6

Li Y, Zhang P, Du Q et al (2011) Adsorption of fluoride from aqueous solution by graphene. J Colloid Interface Sci 363:348–354. https://doi.org/10.1016/j.jcis.2011.07.032

Li Y, Du Q, Wang J et al (2013) Defluoridation from aqueous solution by manganese oxide coated graphene oxide. J Fluor Chem 148:67–73. https://doi.org/10.1016/j.jfluchem.2013.01.028

Liu H, Deng S, Li Z, Yu G, Huang J (2010) Preparation of Al–Ce hybrid adsorbent and its application for defluoridation of drinking water. J Hazard Mater 179:424–430. https://doi.org/10.1016/j.jhazmat.2010.03.021

McKay G, Otterburn MS, Sweeney AG (1981) Surface mass transfer processes during colour removal from effluent using silica. Water Res 15:327–331. https://doi.org/10.1016/0043-1354(81)90036-1

Meenakshi, Maheshwari RC (2006) Fluoride in drinking water and its removal. J Hazard Mater 137:456–463. https://doi.org/10.1016/j.jhazmat.2006.02.024

Mohan S, Kumar V, Singh DK, Hasan SH (2016a) Synthesis and characterization of rGO/ZrO $_2$ nanocomposite for enhanced removal of fluoride from water: kinetics, isotherm, and thermodynamic modeling and its adsorption mechanism. RSC Adv 6:87523–87538. https://doi.org/10.1039/C6RA15460C

Mohan S, Kumar V, Singh DK, Hasan SH (2016b) Synthesis and characterization of rGO/ZrO $_2$ nanocomposite for enhanced removal of fluoride from water: kinetics, isotherm, and thermodynamic modeling and its adsorption mechanism. RSC Adv 6:87523–87538. https://doi.org/10.1039/C6RA15460C

Mohammadian S, Ghanemi K, Nikpour Y (2016) Competitive adsorption of phthalate esters on marine surface sediments: kinetic, thermodynamic, and environmental considerations. Environ Sci Pollut Res 23:24991–25002. https://doi.org/10.1007/s11356-016-7723-9

Mukhopadhyay K, Ghosh A, Das SK, Show B, Sasikumar P, Chand Ghosh U (2017b) Synthesis and characterisation of cerium(IV)-incorporated hydrous iron(III) oxide as an adsorbent for fluoride removal from water. RSC Adv 7:26037–26051. https://doi.org/10.1039/c7ra00265c

Novoselov KS (2004) Electric Field Effect in Atomically Thin Carbon Films. Science 306:666–669. https://doi.org/10.1126/science.1102896

Podder MS, Majumder CB (2016) Application of granular activated carbon/MnFe2O4 composite immobilized on C. glutamicum MTCC 2745 to remove As(III) and As(V): Kinetic, mechanistic and thermodynamic studies. Spectrochim Acta A Mol Biomol Spectrosc 153:298–314. https://doi.org/10.1016/j.saa.2015.08.022

Ranjan D, Talat M, Hasan SH (2009) Biosorption of arsenic from aqueous solution using agricultural residue 'rice polish'. J Hazard Mater 166:1050–1059. https://doi.org/10.1016/j.jhazmat.2008.12.013

Reichenberg D (1953) Properties of Ion-Exchange Resins in Relation to their Structure. III. Kinetics of Exchange. J Am Chem Soc 75:589–597. https://doi.org/10.1021/ja01099a022

Saha I, Ghosh A, Nandi D et al (2015) ß-Cyclodextrin modified hydrous zirconium oxide: Synthesis, characterization and defluoridation performance from aqueous solution. Chem Eng J 263:220–230. https://doi.org/10.1016/j.cej.2014.11.039

Sharma YC, Weng CH (2007) Removal of chromium(VI) from water and wastewater by using riverbed sand: Kinetic and equilibrium studies. J Hazard Mater 142:449–454. https://doi.org/10.1016/j.jhazmat.2006.08.078

Singh DK, Mohan S, Kumar V, Hasan SH (2016) Kinetic, isotherm and thermodynamic studies of adsorption behaviour of CNT/CuO nanocomposite for the removal of As(iii) and As(v) from water. RSC Adv 6:1218–1230. https://doi.org/10.1039/C5RA20601D

Singh DK, Kumar V, Mohan S, Hasan SH (2017) Polylysine Functionalized Graphene Aerogel for the Enhanced Removal of Cr(VI) through Adsorption: Kinetic, Isotherm, and Thermodynamic Modeling of the Process. J Chem Eng Data 62:1732–1742. https://doi.org/10.1021/acs.jced.7b00188

Tang D, Zhang G (2016) Efficient removal of fluoride by hierarchical Ce–Fe bimetal oxides adsorbent: Thermodynamics, kinetics and mechanism. Chem Eng J 283:721–729. https://doi.org/10.1016/j.cej.2015.08.019

Tomar V, Prasad S, Kumar D (2013) Adsorptive removal of fluoride from water samples using Zr–Mn composite material. Microchem J 111:116–124. https://doi.org/10.1016/j.microc.2013.04.007

Wan Z, Wang J (2016) Ce-Fe-reduced graphene oxide nanocomposite as an efficient catalyst for sulfamethazine degradation in aqueous solution. Environ Sci Pollut Res 23:18542–18551. https://doi.org/10.1007/s11356-016-7051-0

Wen S, Wang Y, Dong S (2015) Performance and characteristics of fluoride adsorption using nanomagnetite graphite-La adsorbent. RSC Adv 5:89594–89602. https://doi.org/10.1039/c5ra15215a

Zhang K, Wu S, Wang X, He J, Sun B, Jia Y, Luo T, Meng F, Jin Z, Lin D, Shen W, Kong L, Liu J (2015) Wide pH range for fluoride removal from water by MHS-MgO/MgCO3 adsorbent: Kinetic, thermodynamic and mechanism studies. J Colloid Interface Sci 446:194–202. https://doi.org/10.1016/j.jcis.2015.01.049

Zhang C, Li Y, Wang T-J, Jiang Y, Fok J (2017) Synthesis and properties of a high-capacity iron oxide adsorbent for fluoride removal from drinking water. Appl Surf Sci 425:272–281. https://doi.org/10.1016/j.apsusc.2017.06.159

Zhao B, Zhang Y, Dou X, Wu X, Yang M (2012a) Granulation of Fe–Al–Ce trimetal hydroxide as a fluoride adsorbent using the extrusion method. Chem Eng J 185–186:211–218. https://doi.org/10.1016/j.cej.2012.01.085

Zhao B, Zhang Y, Dou X, Wu X, Yang M (2012b) Granulation of Fe-Al-Ce trimetal hydroxide as a fluoride adsorbent using the extrusion method. Chem Eng J 185-186:211–218. https://doi.org/10.1016/j.cej.2012.01.085

Zhu J, Lin X, Wu P, Zhou Q, Luo X (2015) Fluoride removal from aqueous solution by Al(III)–Zr(IV) binary oxide adsorbent. Appl Surf Sci 357:91–100. https://doi.org/10.1016/j.apsusc.2015.09.012